AD-A068 179 SYRACUSE UNIV NY DEPT OF ELECTRICAL AND COMPUTER EN--ETC F/G 11/4
THIN-WIRE METHODS FOR ELECTROMAGNETIC PROBLEMS INVOLVING ADVANC--ETC(U)
FEB 79 A T ADAMS, C CHANG F30602-78-C-0083

UNCLASSIFIED RADC-TR-79-18 NL

| OF |
AD
A068179

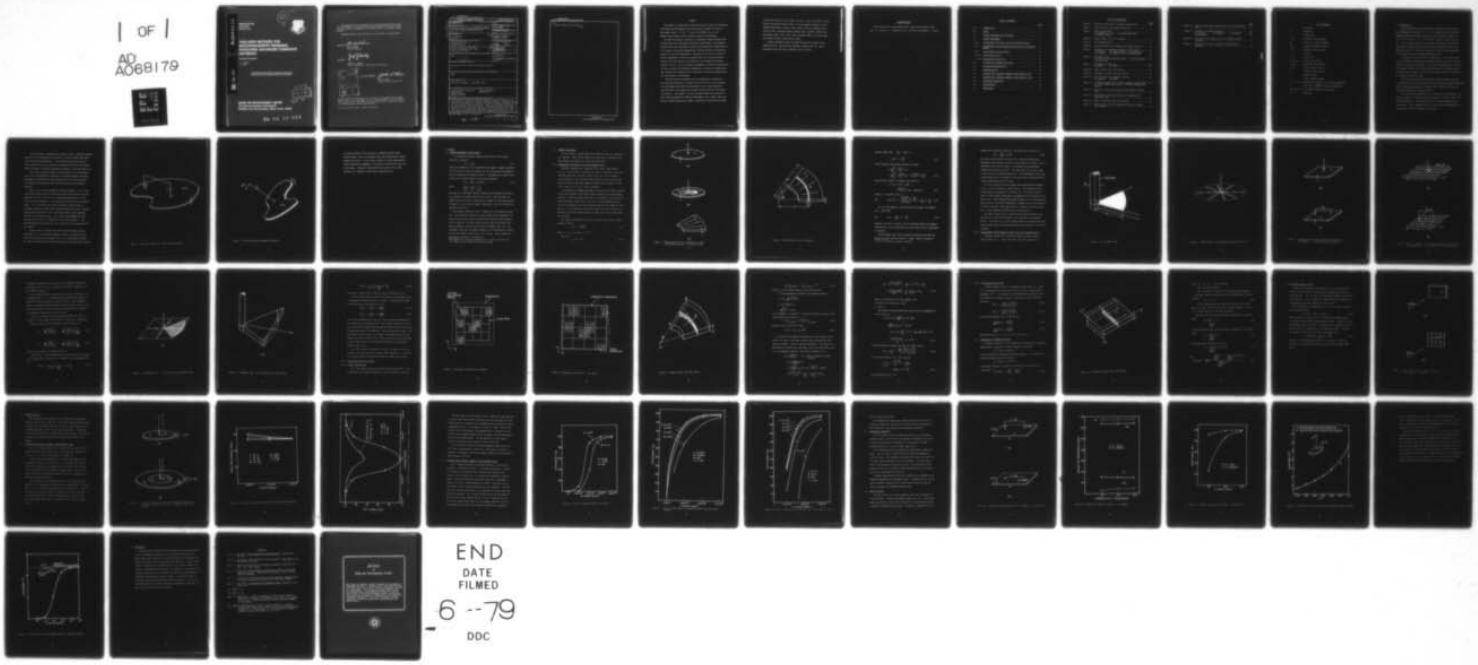

END
DATE
FILMED
6 -79
DDC

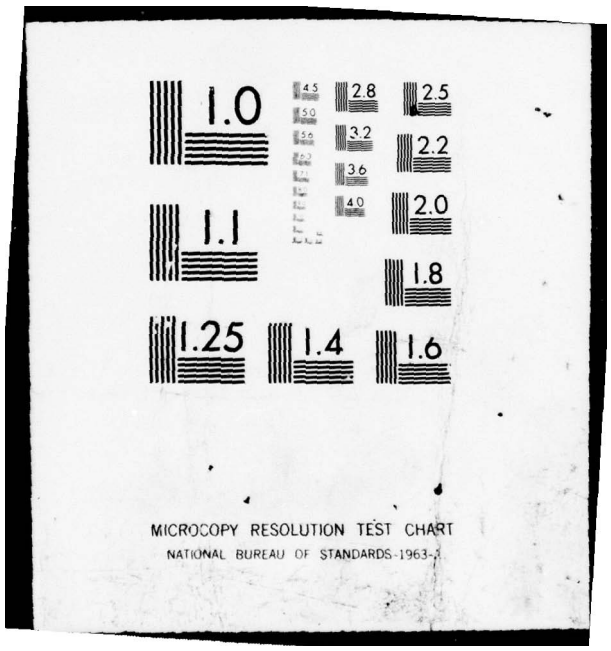
1.0
1.1
1.25
1.4
1.6
1.8
2.0
2.2
2.5
2.8
3.2
3.6
4.0
4.5
5.0
5.6
6.3
MICROCOPY RESOLUTION TEST CHART
NATIONAL BUREAU OF STANDARDS-1963-A

RADC-TR-79-18
Phase Report
February 1979

THIN-WIRE METHODS FOR ELECTROMAGNETIC PROBLEMS INVOLVING ADVANCED COMPOSITE MATERIALS

Syracuse University

A. T. Adams
C. Chang

ROME AIR DEVELOPMENT CENTER
Air Force Systems Command
Griffiss Air Force Base, New York 13441

This report has been reviewed by the RADC Information Office (OI) and is releasable to the National Technical Information Service (NTIS). At NTIS it will be releasable to the general public, including foreign nations.

RADC-TR-79-18 has been reviewed and is approved for publication.

APPROVED: Jacob Scherer

JACOB SHERER
Project Engineer

APPROVED: Joseph J. Naresky

JOSEPH J. NARESKY
Chief, Reliability & Compatibility Division

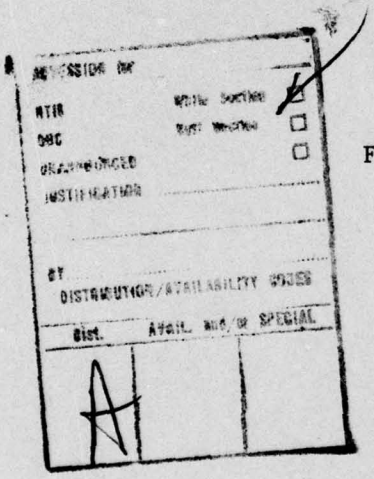

FOR THE COMMANDER: John P. Huss

JOHN P. HUSS
Acting Chief, Plans Office

If your address has changed or if you wish to be removed from the RADC mailing list, or if the addressee is no longer employed by your organization, please notify RADC (RBC), Griffiss AFB NY 13441. This will assist us in maintaining a current mailing list.

Do not return this copy. Retain or destroy.

UNCLASSIFIED

SECURITY CLASSIFICATION OF THIS PAGE (When Data Entered)

REPORT DOCUMENTATION PAGE	READ INSTRUCTIONS BEFORE COMPLETING FORM
1. REPORT NUMBER: RADC-TR-79-18	2. GOVT ACCESSION NO. / 3. RECIPIENT'S CATALOG NUMBER
4. TITLE (and Subtitle): THIN-WIRE METHODS FOR ELECTROMAGNETIC PROBLEMS INVOLVING ADVANCED COMPOSITE MATERIALS	5. TYPE OF REPORT & PERIOD COVERED: Phase Report Oct 77 – Sep 78
	6. PERFORMING ORG. REPORT NUMBER: N/A
7. AUTHOR(s): A. T. Adams, C. Chang	8. CONTRACT OR GRANT NUMBER(s): F30602-78-C-0083, F30602-75-C-0121
9. PERFORMING ORGANIZATION NAME AND ADDRESS: Syracuse University, ECE Department (Dept. of Elec. & Computer Eng.), Syracuse NY 13210	10. PROGRAM ELEMENT, PROJECT, TASK AREA & WORK UNIT NUMBERS: 62702F, 23380304
11. CONTROLLING OFFICE NAME AND ADDRESS: Rome Air Development Center (RBC), Griffiss AFB NY 13441	12. REPORT DATE: February 1979
	13. NUMBER OF PAGES: 58
14. MONITORING AGENCY NAME & ADDRESS (if different from Controlling Office): Same	15. SECURITY CLASS. (of this report): UNCLASSIFIED
	15a. DECLASSIFICATION DOWNGRADING SCHEDULE: N/A

16. DISTRIBUTION STATEMENT (of this Report)

Approved for public release; distribution unlimited.

17. DISTRIBUTION STATEMENT (of the abstract entered in Block 20, if different from Report)

Same

18. SUPPLEMENTARY NOTES

RADC Project Engineer: Jacob (NMI) Sherer

19. KEY WORDS (Continue on reverse side if necessary and identify by block number)

Advanced Composite Materials
Conductivity
Method of Moments
Antenna Thin Wire
Antenna Efficiency
Back-scatter

20. ABSTRACT (Continue on reverse side if necessary and identify by block number)

This report describes loaded thin-wire models for the representation of the electromagnetic properties of advanced composite materials. Techniques are described for the treatment of thin-wire antennas over advanced composite surfaces and for back-scattering from composites. Special techniques are required for the representation of attachment points. Skin effect is taken into account. Antenna efficiency and gain are computed. The results indicate that a small metal "pad" at attachment points may significantly improve efficiency. Far field beam patterns may remain essentially unchanged as efficiency or back-

DD FORM 1 JAN 73 1473 EDITION OF 1 NOV 65 IS OBSOLETE

UNCLASSIFIED

SECURITY CLASSIFICATION OF THIS PAGE (When Data Entered)

scatter varies over a wide range.

PREFACE

This effort was conducted by Syracuse University under the sponsorship of the Rome Air Development Center Post-Doctoral Program for Rome Air Development Center. Dr. Roy F. Stratton, RADC/RBCT, was project engineer and provided overall technical direction and guidance.

The RADC Post-Doctoral Program is a cooperative venture between RADC and some sixty-five universities eligible to participate in the program. Syracuse University (Department of Electrical Engineering), Purdue University (School of Electrical Engineering), Georgia Institute of Technology (School of Electrical Engineering), and State University of New York at Buffalo (Department of Electrical Engineering) act as prime contractor. schools with other schools participating via sub-contracts with prime schools. The U.S. Air Force Academy (Department of Electrical Engineering), Air Force Institute of Technology (Department of Electrical Engineering), and the Naval Post Graduate School (Department of Electrical Engineering) also participate in the program.

The Post-Doctoral Program provides an opportunity for faculty at participating universities to spend up to one year full time on exploratory development and problem-solving efforts with the post-doctorals splitting their time between the customer location and their educational institutions. The program is totally customer-funded with current projects being undertaken for Rome Air Development Center (RADC), Space and Missile Systems Organization (SAMSO), Aeronautical System Division (ASD),

Electronics Systems Division (ESD), Air Force Avionics Laboratory (AFAL), Foreign Technology Division (FTD), Air Force Weapons Laboratory (AFWL), Armament Development and Test Center (ADTC), Air Force Communications Service (AFCS), Aerospace Defense Command (ADC), HQ USAF, Defense Communications Agency (DCA), Navy, Army, Aerospace Medical Division (AMD), and Federal Aviation Administration (FAA).

Further information about the RADC Post-Doctoral Program can be obtained from Mr. Jacob Scherer, RADC/RBC, Griffiss AFB, NY, 13441, telephone Autovon 587-2543, Commercial (315) 330-2543.

ACKNOWLEDGMENTS

The authors wish to acknowledge useful suggestions and advice from Drs. J. A. Allen, R. F. Harrington, Roy F. Stratton, and Bradley J. Strait.

TABLE OF CONTENTS

LIST OF ILLUSTRATIONS

List of Symbols

λ	= wavelength
t	= thickness
σ	= conductivity
z, z_ℓ	= impedance, load impedance
R_i	= Real part of input impedance
R_{eq}	= equivalent lumped resistance
v, v'	= voltage, applied voltage
i, I	= current
r_a, a	= wire radius
R, R_1, R_2	= circular disk radii
r_x, r_y	= equivalent sector radius
J', J_ρ	= volume current density
E	= electric field intensity
N	= number of wires
ℓ	= wire or segment length
$\gamma = \alpha + j\ \beta$	= propagation constant ($\alpha=\beta$ for good conductors)
δ	= skin depth = $\sqrt{2/\omega\mu\sigma}$ (for good conductors)
W_ℓ, W_R, W_t	= dissipated, radiated, input power
A_e	= echo area

I. Introduction

Thin-wire methods have proven useful in treating a wide variety of electromagnetic problems [1] - [3]. At present there are many well-documented computer programs available for the treatment of thin wires ($\ell >> a$, $a << \lambda$, where a, ℓ are antenna radius, length, respectively) [1] - [3]. Some of these include the most general orientation (arbitrarily skewed wires), permit arbitrary excitation and loading, and take junctions into account. The thin wire codes are the most highly developed and well-tested of all the method-of-moments codes.

In addition to treating thin-wire geometries, the thin-wire codes are also capable of approximately treating conducting surfaces, which are modeled as wire-grid structures. The wire-grid representation is useful in computing radiation and scattering characteristics. Numerous geometries have been treated by the wire-grid technique, which can be applied to surfaces of arbitrary shape.

The thin-wire codes can be extended by lumped loading techniques to approximately treat some problems involving advanced composite materials such as radiating properties of antennas over a composite surface and back-scattering from a composite surface.

The thin-wire representation of a surface has its limitations; one would not expect to obtain accurate near fields or interior fields from this representation. The reactive part of the input impedance may not be accurate. These limitations apply to all wire-grid representations with perfect as well as imperfect conductors.

The key problem in applying the thin-wire codes to advanced composite materials is the computation and location of various lumped loads added to the wire-grid representation. These loads must take into account the junctions of wires and surfaces (attachment points) and skin effect. Some of the basic techniques have been described in a previous report [4].

This report describes loaded thin-wire models for the representation of the electromagnetic properties of advanced composite materials. Techniques are developed for the representation of thin-wire antennas over composite ground planes and for back-scattering from composite surfaces.

Figs. 1 and 2 show the general problems considered. Fig. 1 shows a thin-wire antenna, which is driven and loaded at arbitrary points and attached at points "a" and "b" to a composite ground plane of conductivity $\sigma(r)$ and thickness t. The conductivity may vary over the ground plane. It is shown later that highly conductive "pads" located at attachment points may significantly improve antenna efficiency. Antenna characteristics desired are far field beam patterns, input impedance, efficiency, and directive gain. Fig. 2 shows electromagnetic fields incident upon a surface of conductivity $\sigma(r)$ and thickness t. The back-scattering cross section and the scattered far field beam patterns are desired.

Several types of problems have been treated including antenna problems (Fig. 1) with azimuthal symmetry and with rectangular ground planes and back-scattering problems (Fig. 2) for rectangular surfaces. The results indicate that antenna efficiency may be significantly reduced

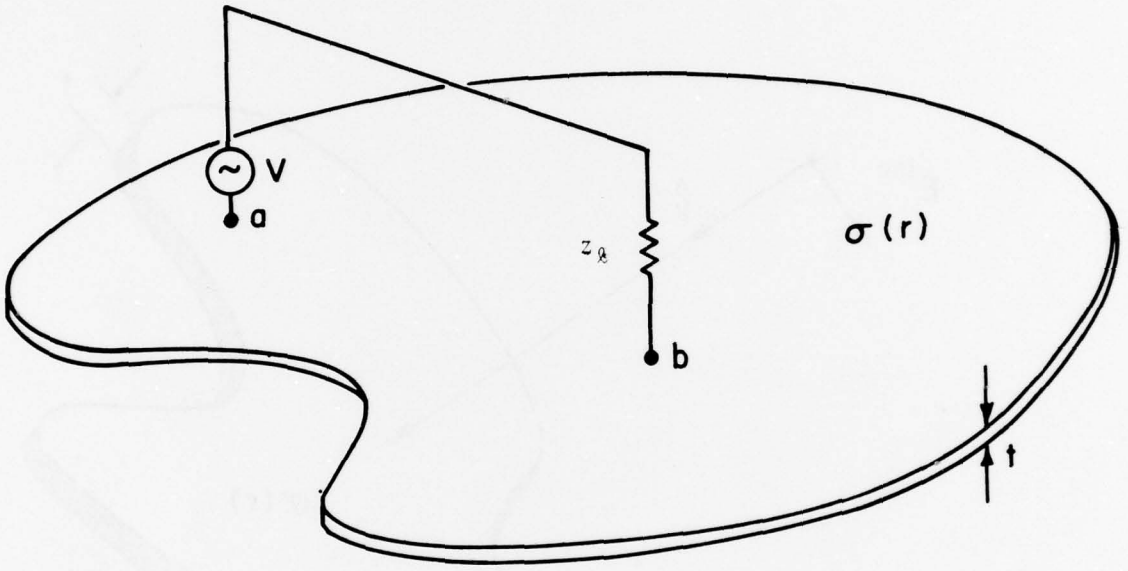

Figure 1. Thin-wire Antenna over a Composite Ground Plane

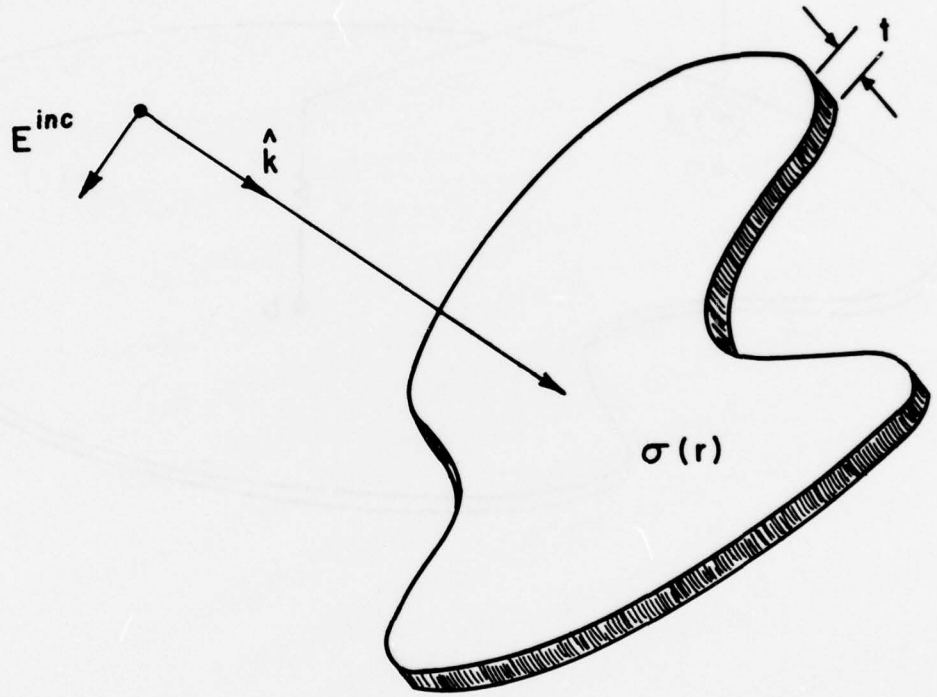

Figure 2. Back-scattering from Composite Material

for some problems by the presence of a composite ground plane. Antenna "pads" near the attachment points may significantly improve antenna efficiency. In some cases, antenna far field beam patterns remain essentially unchanged as efficiency or back-scatter vary over a wide range. Therefore, beam pattern data alone is not a good indicator of antenna or back-scatter characteristics.

2.0 THEORY

2.1 LOADING TECHNIQUES FOR THIN WIRES

In the method-of-moments formulation for thin wires a matrix equation is obtained:

$$[v] = [z][i] \tag{2-1}$$

where the elements of [v] are generalized voltages (weighted integrals of the electric field), the elements of [z] are generalized impedances, and [i] represents the unknown currents. The addition of lumped loads to the wire structure results in the matrix equation

$$[v'] = \left[[z] + [z_\ell]\right] [i] \tag{2-2}$$

where $$\left[z_\ell\right] = \begin{bmatrix} z_{\ell 1} & & 0 \\ & \ddots & \\ 0 & & z_{\ell n} \end{bmatrix}$$

and where [v'] represents applied voltage and the diagonal* load matrix $[z_\ell]$ contains the lumped loads (see [1], [3]). Thus the effect of lumped loads is merely to replace total voltages [v] with known applied voltages [v'] and to add a diagonal load matrix $[z_\ell]$ to the generalized impedance matrix [z].

The essential problem is thus to compute the load impedance matrix $[z_\ell]$. The conduction current $\sigma \underline{E}$ is much larger than displacement current $j\omega\varepsilon \underline{E}$ for typical values of interest and thus the load impedances will be resistive. The skin effect must be taken into account since typical composite thickness may be many skin depths (see [5]). The attachment point must be modeled properly so as to enforce the radially outward (or inward) current flow in its vicinity. These effects are considered in sections 2.2 through 2.4.

*The load matrix is purely diagonal only in special cases [1], [3]. for example, pulse functions and point matching.

2.2 CURRENT FLOW MODELS

In this section, loading models for different types of current flow are examined. These include models for radial flow, rectangular flow and current flow taking into account the skin effect.

2.2.1 Loading Model for Radial Flow and Attachment Points

Consider a monopole on a composite disk, such as that shown in Fig. 3a. In this case, current flow is radial. The disk is first subsectioned into small sectors as shown in Fig. 3b. Fig. 3c shows a typical subsector. We then model each subsector with a wire and load each wire with an equivalent lumped resistance which accounts for the finite conductivity of the composite material.

To calculate the loading resistance we first let the current flowing on the wire be equal to the total current flowing on the corresponding subsector. Then the loading resistance is calculated as that which will produce the same voltage drop as that over a corresponding subsector. For the low frequency case (skin depth much greater than composite thickness t), it is assumed that the current flows uniformly throughout the thickness of the disk (modifications are made later to take skin depth into account).

The volume current density J_ρ in a subsector (Fig. 4) may be represented as follows:

$$J_\rho(\rho) = \frac{\rho_1 J(\rho_1)}{\rho} \tag{2-3}$$

where ρ, ρ_1, ρ_2 are shown in Fig. 4.

And since

$$\underline{J} = \sigma \underline{E} = -\sigma \nabla v \tag{2-4}$$

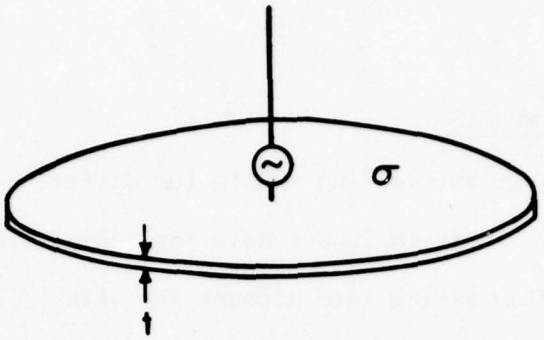

(a)

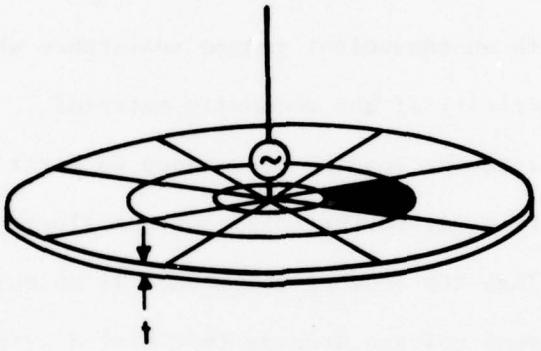

(b)

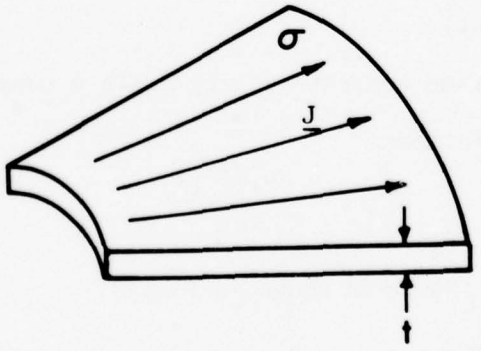

(c)

Figure 3. Radial Current Flow (a) Monopole on a Disk
(b) Subsectional Model (c) Typical Sector

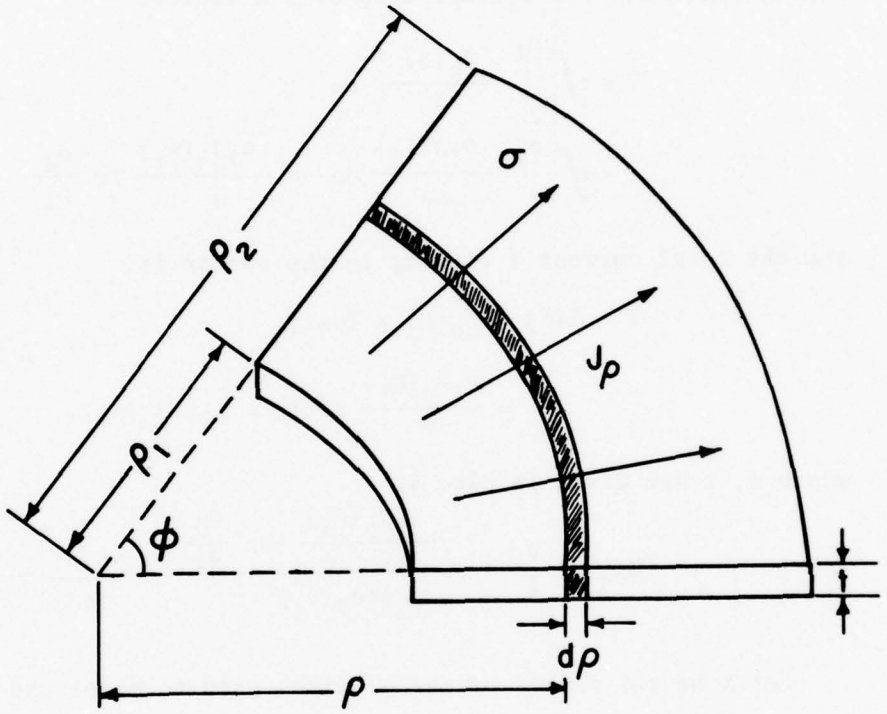

Figure 4. Radial Current Flow on a Subsector

and for radial flow $\frac{\partial}{\partial \phi} = \frac{\partial}{\partial z} = 0$

$$\therefore \quad J_\rho(\rho) = -\sigma \frac{\partial v}{\partial \rho} \tag{2-5}$$

Now we calculate the voltage drop over a sector:

$$V = +\int_{\rho_2}^{\rho_1} \frac{J_\rho(\rho)}{\sigma} d\rho$$

$$= +\int_{\rho_2}^{\rho_1} \frac{\rho_1 J(\rho_1)}{\rho\sigma} d\rho = \frac{\rho_1 J_\rho(\rho_1)}{\sigma} \ell n \frac{\rho_2}{\rho_1} \tag{2-6}$$

and the total current I flowing in the sector is

$$I = I(\rho) = J_\rho(\rho) \times (\rho\phi t)$$

$$= \frac{\rho_1 J_\rho(\rho_1)}{\rho} \times \rho\phi t = \rho_1 \phi t J_\rho(\rho_1) \tag{2-7}$$

where ϕ, t are given in Fig. 4.

and $$R_{eq}^* \equiv \frac{V}{I} = \frac{\frac{\rho_1 J_\rho(\rho_1)}{\sigma} \ell n \frac{\rho_2}{\rho_1}}{\rho_1 \phi t J_\rho(\rho_1)} = \frac{1}{\sigma\phi t} \ell n \frac{\rho_2}{\rho_1} \tag{2-8}$$

Let N be the number of radial wires used to model the composite disk. Then $\phi = \frac{2\pi}{N}$

and $$R_{eq} = \frac{N}{\sigma t 2\pi} \ell n \frac{\rho_2}{\rho_1} \tag{2-9}$$

Equation (2-9) can, of course, also be obtained directly by standard techniques for static resistance; for later cases the full development is required.

The attachment point can be treated by taking into account the radius "a" of the monopole antenna. Figure 5 shows the monopole

* Req is the equivalent lumped resistance.

antenna and a bordering subsector. The equivalent resistance is

$$R_{eq} = \frac{N}{\sigma t 2\pi} \ell n \frac{\rho_2}{a} \qquad (2\text{-}10)$$

Note that the equivalent resistance for a subsector bordering an attachment point depends critically on the actual wire radius. This is reasonable since the wire radius "a" determines the "bottleneck" through which current must flow. The high value of resistance leads to high losses for bordering subsectors. This corresponds to the high losses expected for a resistance in the near field of an antenna where reactive power density may be large.

All load resistances are now known and the monopole-disk problem of Fig. 3a may be modeled as shown in Fig. 6, the resistance values being computed by equations (2-9) and (2-10). The entire system of wires is subsectioned, subsections are numbered, and the diagonal load matrix $[z_\ell]$ is thus known, where typical element $z_{\ell i}$ is the appropriate load resistance for the i^{th} subsection. Currents [i] are then computed by matrix inversion. Then beam patterns, efficiency, directive gain, etc., can be computed by further matrix operations [3].

The case of purely radial current flow has been considered first because of its direct relationship to the treatment of attachment points. In section 2.2.2, a more general model is considered involving radial current flow near attachment points and rectangular current flow elsewhere.

2.2.2 Loading Model for Rectangular Current Flow and Attachment Points

Consider antennas over rectangular composite ground planes as shown in Figs. 7a, c. Again, thin wires are used to model the

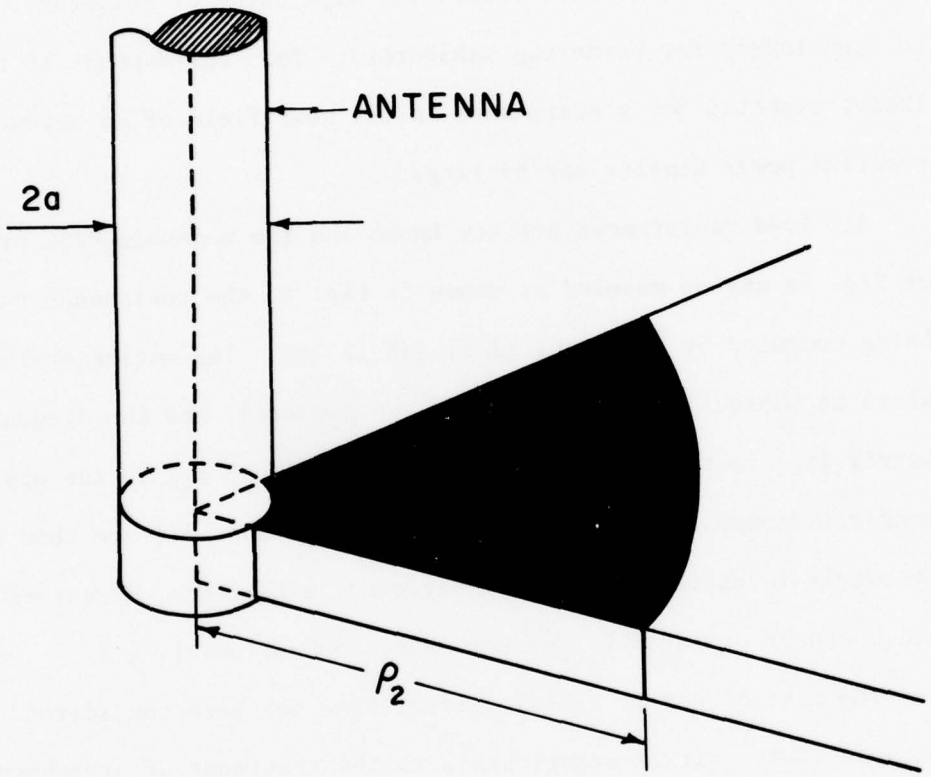

Figure 5. An Attachment Point

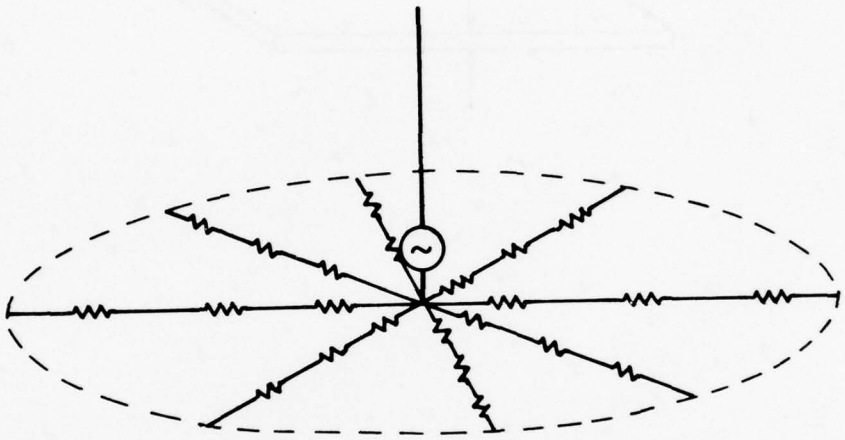

Figure 6. Thin-wire Model of the Monopole and Disk of Figure 3a

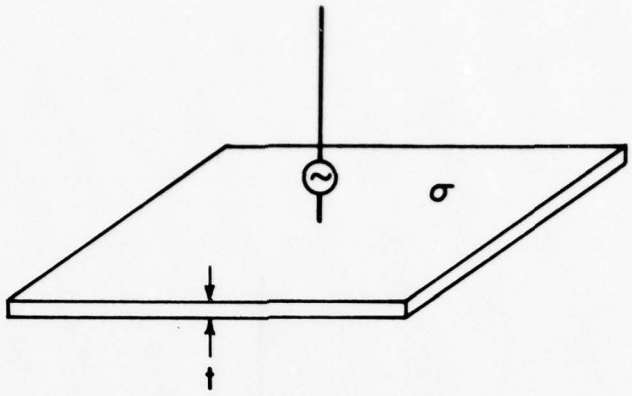

(a)

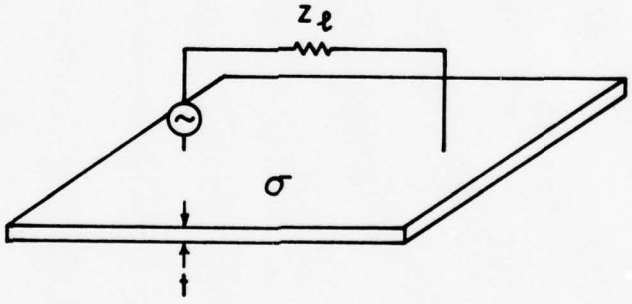

(c)

Figure 7. Antennas over Rectangular Composite Ground Planes
(a) monopole (c) transmission line antenna

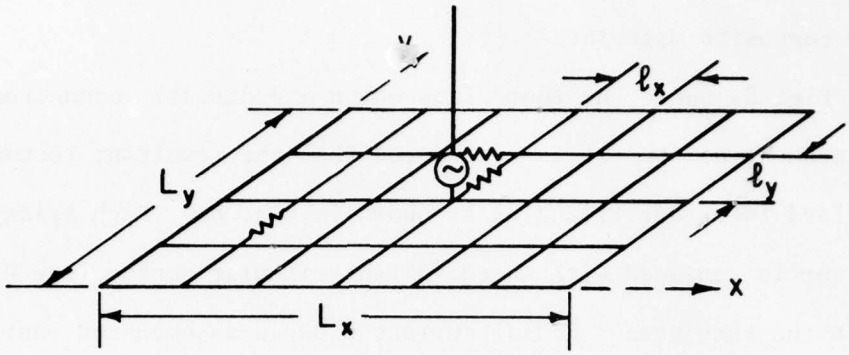

(b)

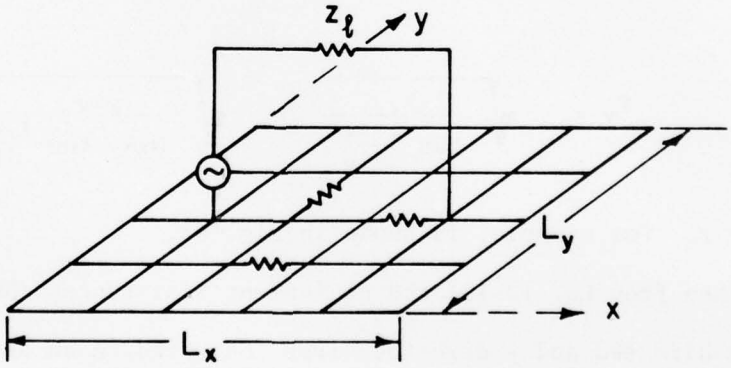

(d)

Figure 7. (part 2) Antennas over Rectangular Composite Ground Planes
(b) monopole model (d) transmission line antenna model

rectangular ground plane and the wires are loaded with equivalent resistances (Figs. 7b, d) to account for the finite conductivity of the composite material.

Fig. 8a shows the four wires which are directly connected to an attachment point. It is considered that the resultant rectangle is divided into four triangles as shown in Fig. 8a. Each triangular sector is replaced with an equivalent circular sector (see Figs. 8a, b) with the same area. Radial current flow is assumed and resistances are computed by equations (2-10), as follows:

Let Lx, Ly be sides of the rectangular ground plane (Fig. 7c) and let Nx, Ny be number of subsections for each side, respectively.

Radii r_x, and r_y of the equivalent circular sectors are

$$r_x = \sqrt{\frac{\ell_x \ell_y}{\tan^{-1}\frac{\ell_y}{\ell_x}}} = \sqrt{\frac{L_x L_y}{N_x N_y \tan^{-1}\frac{L_y N_x}{L_x N_y}}} \qquad (2\text{-}11)$$

$$r_y = \sqrt{\frac{\ell_x \ell_y}{\tan^{-1}\frac{\ell_x}{\ell_y}}} = \sqrt{\frac{L_x L_y}{N_x N_y \tan^{-1}\frac{L_x N_y}{L_y N_x}}} \qquad (2\text{-}12)$$

where r_x, for example, is shown in Fig. 8b.

Then from Eq. (2-10) the equivalent resistances $(Req)_x$ and $(Req)_y$ for x-directed and y-directed wires connected to an attachment point are

$$(R_{eq})_x = \frac{1}{2\sigma t \tan^{-1}\frac{L_y N_x}{L_x N_y}} \ell n \frac{r_x}{r_a} \qquad (2\text{-}13)$$

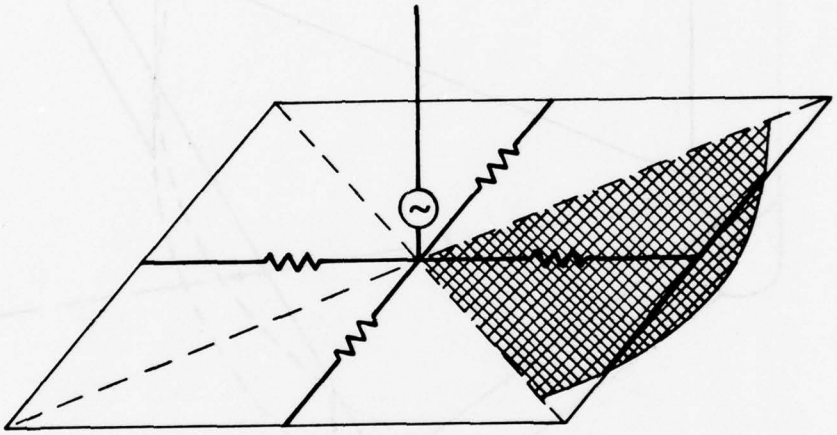

(a)

Figure 8. Attachment Point (a) wires near the attachment point

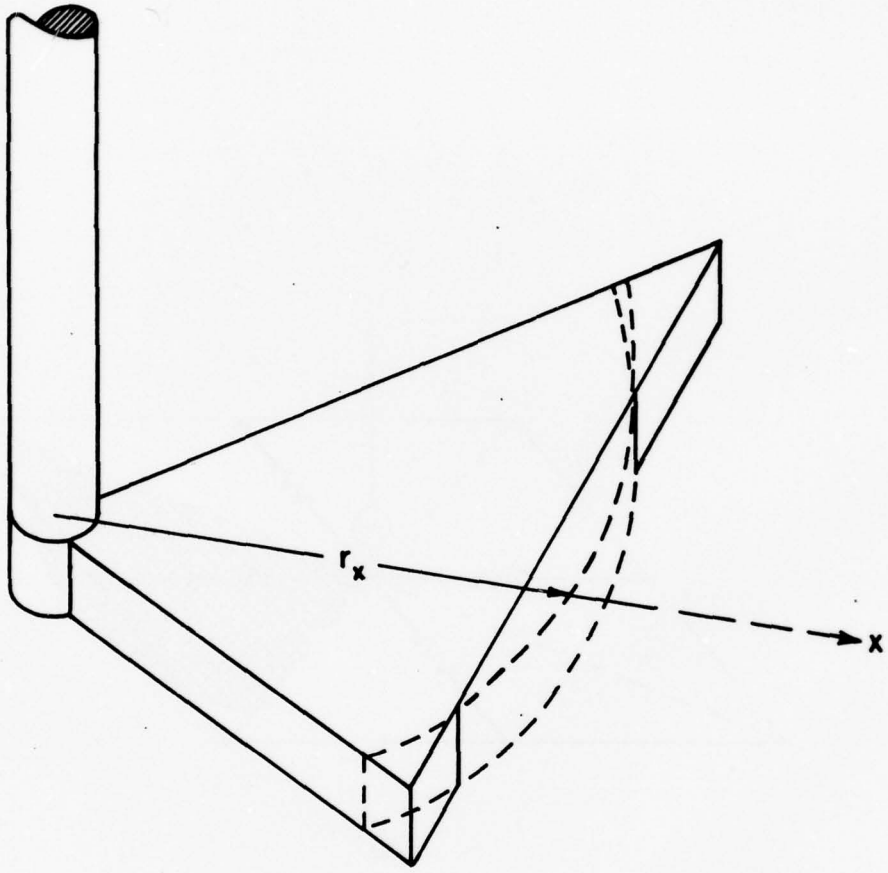

(b)

Figure 8. Attachment Point (b) the equivalent circular sector

$$(R_{eq})_y = \frac{1}{2\sigma t \tan^{-1}\frac{L_x N_y}{L_y N_x}} \ln \frac{r_y}{r_a} \qquad (2\text{-}14)$$

Thus radial current flow is enforced near the attachment point.

For all other wires not directly connected to an attachment point, a rectangular current flow model is assumed. Equivalent resistances for x-directed and y-directed wires are

$$(R_{eq})_x = \frac{\ell_x}{\sigma t \ell_y} = \frac{L_x N_y}{\sigma t L_y N_x} \qquad (2\text{-}15)$$

$$(R_{eq})_y = \frac{\ell_y}{\sigma t \ell_x} = \frac{L_y N_x}{\sigma t L_x N_y} \qquad (2\text{-}16)$$

for the low frequency case. Figs. 9a, b show typical representations of a surface by a rectangular grid. The currents flowing in the wire grid sections each represent an equivalent surface current flowing over an equivalent area of the composite. Equivalent areas are shown. The equivalent resistors $(R_{eq})_x$, for example, are identical for Fig. 9a, whereas the edge resistors of Fig. 9b are twice the value of the others. Typical results show little difference between the two alternative models of Figs. 9a, b.

All of the results in sections 2.2.1 and 2.2.2 apply to the low frequency case (skin depth much greater than thickness t). In section 2.2.3, these results are modified to take skin depth into account.

2.2.3 Loading Models for Skin Effect

2.2.3.1 Radial Current Flow

Fig. (10) shows a typical sector for radial current flow. It is assumed that the current distribution in the z direction is given by

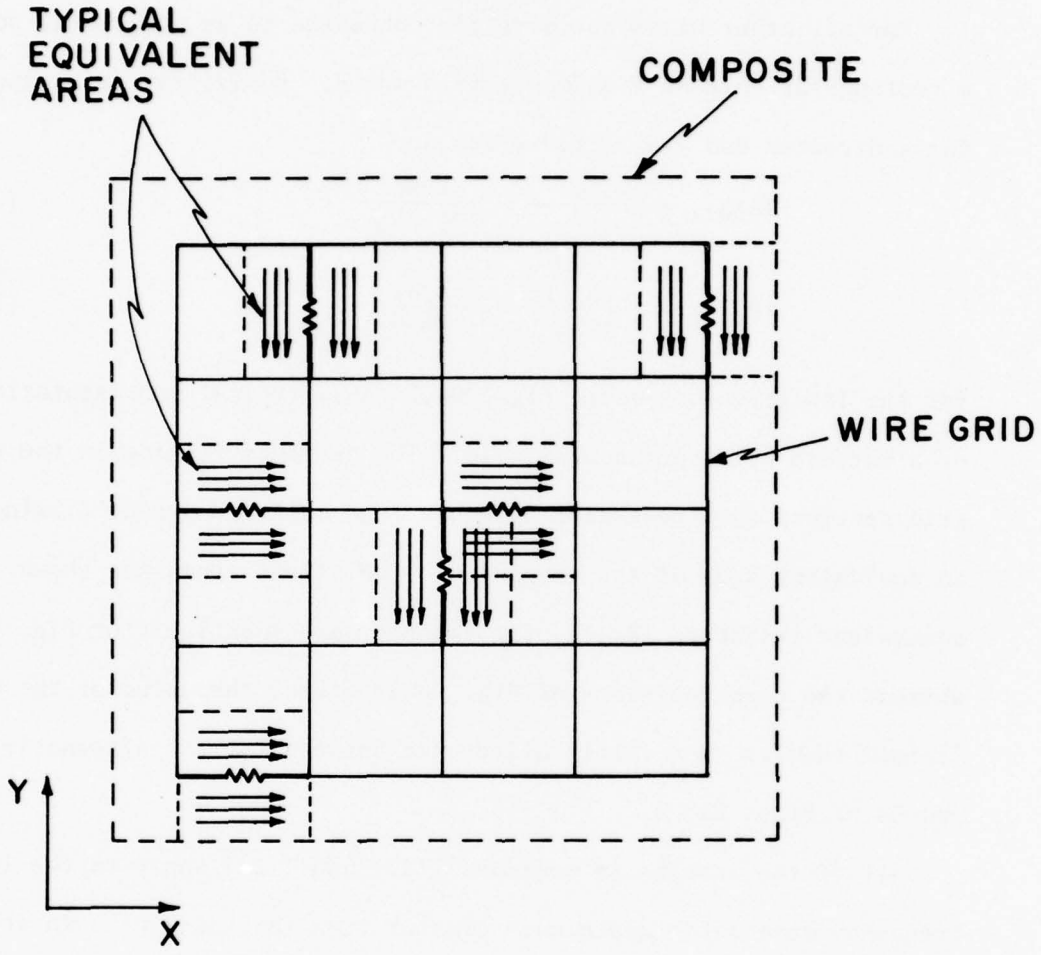

Figure 9. Rectangular Current Flow (a) model 1

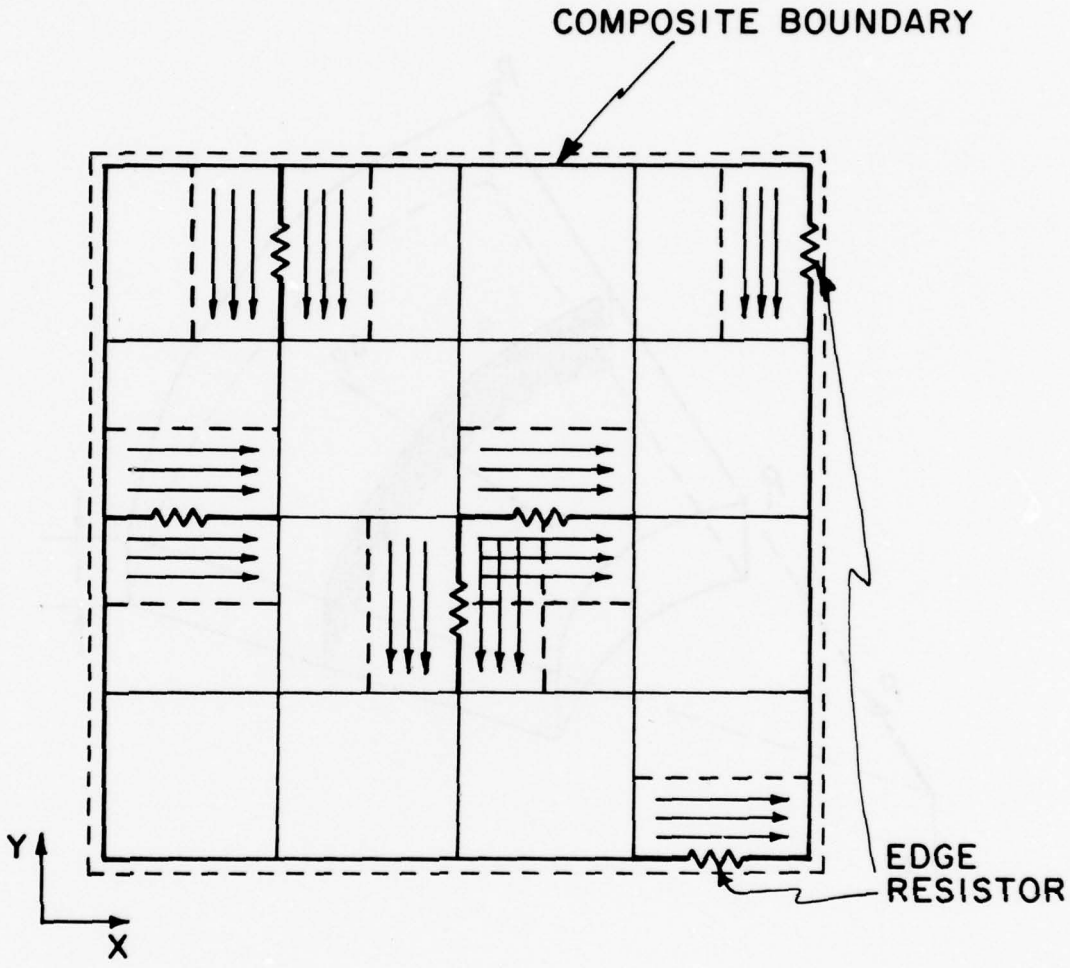

Figure 9. Rectangular Current Flow (b) model 2

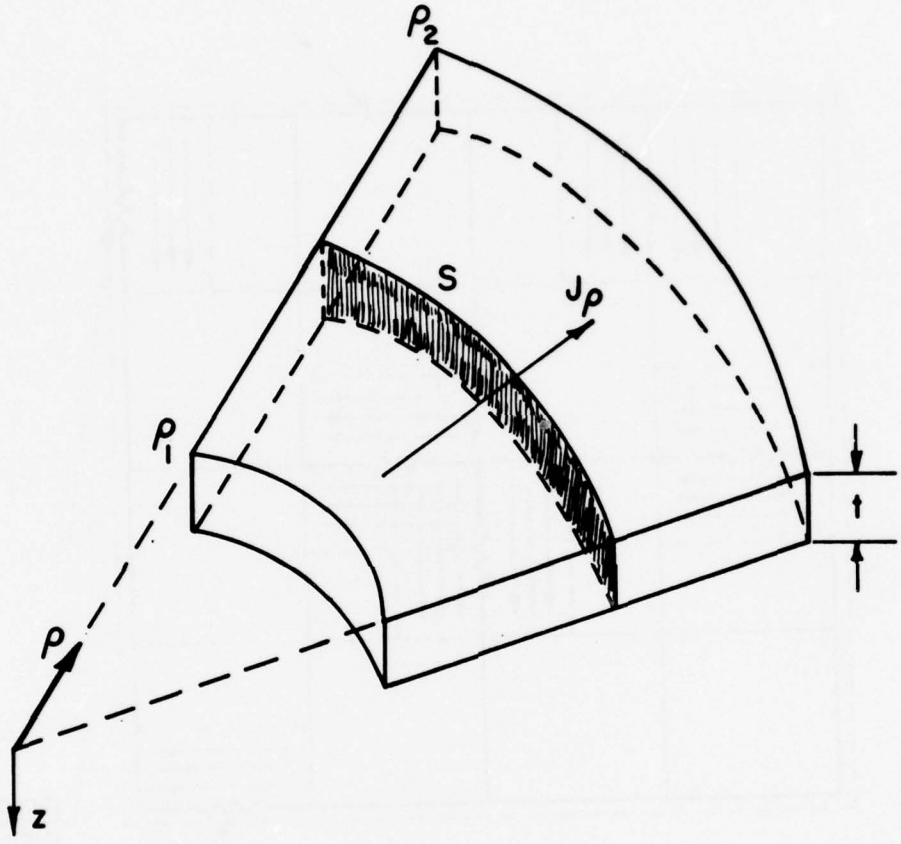

Figure 10. Radial Current Flow (skin effect)

$$J_\rho(z)\Big|_{\rho=\text{const.}} = J_o\Big|_{\rho=\text{ const.}}\ e^{-\gamma z} \qquad (2\text{-}17)$$

where $J_{\rho o}$ is the current density at the surface (z=0)

γ is the propagation constant of the composite material

$$\gamma = \alpha + j\beta = \sqrt{j\omega\mu(\sigma+j\omega\epsilon)}$$

$$\delta = \text{skin depth} = \frac{1}{\alpha}$$

$$= \sqrt{2/\omega\mu\sigma} \quad (\sigma >> \omega\epsilon)$$

It is assumed as in section 2.2.1 that the current variation is the radial direction is given by

$$J(\rho)\Big|_{z=\text{const.}} = \frac{\rho_1 J(\rho_1)}{\rho}\Bigg|_{z=\text{const.}} \qquad (2\text{-}18)$$

Equations (2-17) and (2-18) yield

$$J(\rho,z) = \rho_1 J_o\ (\rho_1)\ \frac{e^{-\gamma z}}{\rho} \qquad (2\text{-}19)$$

To calculate the loading resistance the current flowing on the wire is set equal to the total current flowing through the cross-section as before. Then the loading resistance is calculated to be that which will produce the same ohmic loss as the total ohmic loss in a corresponding subsector. The power dissipated [7] is

$$W_\ell = \text{Re}\iiint \underline{E}\cdot\underline{J}^*\,dv, \text{ where * represents complex conjugate}$$

$$= \frac{1}{\sigma}\iiint \left|\underline{J}\right|^2 dv$$

$$= \frac{1}{\sigma}\iiint \rho_1^2\ \left|J_o(\rho_1)\right|^2\ \frac{\left|e^{-2\gamma z}\right|}{\rho^2}\ \rho\,d\rho\,d\phi\,dz$$

$$= \frac{\rho_1^2\ \left|J_o(\rho_1)\right|^2}{\sigma}\ \Phi\int_{\rho_1}^{\rho_2}\ \frac{d\rho}{\rho}\int_o^t\ e^{-2\alpha z}dz$$

$$W_\ell = \frac{\rho_1^2 \left| J_o(\rho_1) \right|^2 \Phi}{\sigma} \left(\frac{1}{2\alpha}\right) \left[1-e^{-2\alpha t}\right] \ell n \frac{\rho_2}{\rho_1}$$

$$= \frac{2\pi\rho_1^2 \left| J_o(\rho_1) \right|^2}{2\sigma N\alpha} \left(\ell n \frac{\rho_2}{\rho_1}\right)\left[1-e^{-2\alpha t}\right] \qquad (2\text{-}20)$$

where t is the thickness of the composite disk

N is the No. of radial wires used

α = Re (γ).

The current flowing through the cross section is independent of ρ and is given by

$$\left| I \right| = \left| I(\rho) \right| = \iint \left| J(\rho, z) \right| \rho dz d\phi$$

$$= \iint \left| \rho_1 J_o(\rho_1) e^{-\gamma z} \right| dz \, d\phi$$

$$= \Phi\rho_1 \left| J_o(\rho_1) \right| \int_o^t e^{-\alpha z} dz \quad (\text{Since } \left| e^{-\gamma z} \right| = e^{-\alpha z})$$

$$= \frac{\left| J_o(\rho_1) \right| 2\pi\rho_1}{\alpha N} (1 - e^{-\alpha t}) \qquad (2\text{-}21)$$

and the equivalent loading resistance for radial flow is

$$R_{eq} \equiv \frac{W}{|I|^2} = \frac{\alpha N \ell n \frac{\rho_1}{\rho_2} (1-e^{-2\alpha t})}{4\pi\sigma \quad (1-e^{-\alpha t})^2} \qquad (2\text{-}22)$$

For the low frequency case, $\alpha t \geq 0$ and thus

$$\lim_{\alpha t \to 0} R_{eq} = \frac{\alpha N \ell n \frac{\rho_1}{\rho_2}}{4\pi\sigma} \times \frac{2\alpha t}{(\alpha t)^2}$$

$$= \frac{N}{2\pi\sigma t} \ell n \frac{\rho_2}{\rho_1} \qquad (2\text{-}23)$$

which agrees with Eq. (2-9)

2.2.3.2 Rectangular Current Flow

Consider current flow in a rectangular section (Fig. 11). Again it is assumed that the current distribution in the z direction has a dependence $e^{-\gamma z}$. It then follows by straightforward calculation that the equivalent resistances $(R_{eq})_x$ are $(R_{eq})_y$ for x- and y-directed wires are

$$(R_{eq})_x = \frac{\alpha L_x N_y (1-e^{-2\alpha t})}{2\sigma L_y N_x (1-e^{-\alpha t})^2} \tag{2-24}$$

$$(R_{eq})_y = \frac{\alpha L_y N_x (1-e^{-2\alpha t})}{2\sigma L_x N_y (1-e^{-\alpha t})^2} \tag{2-25}$$

For the low frequency case, $\alpha t \geqslant 0$ and thus

$$\lim_{\alpha t \geqslant 0} (R_{eq})_x = \frac{L_x N_y}{\sigma t L_y N_x} \tag{2-26}$$

$$\lim_{\alpha t \geqslant 0} (R_{eq})_y = \frac{L_y N_x}{\sigma t L_x N_y} \tag{2-27}$$

which agrees with Eq. (2-15) and (2-16) respectively.

2.3 CALCULATION OF ANTENNA EFFICIENCY

As noted in section 2.1, the problem of an antenna over a composite ground plane is reduced to a matrix equation of the form

$$[v'] = [[z] + [z_\ell]] \quad [i]$$

once the equivalent resistances have been computed. The currents [i] are then obtained by matrix inversion:

$$[i] = [[z] + [z_\ell]]^{-1} [v'].$$

The antenna efficiency is defined as the ratio of radiated power to input power:

$$\text{Efficiency} = \frac{W_R}{W_t} = \frac{W_t - W_\ell}{W_t} \tag{2-28}$$

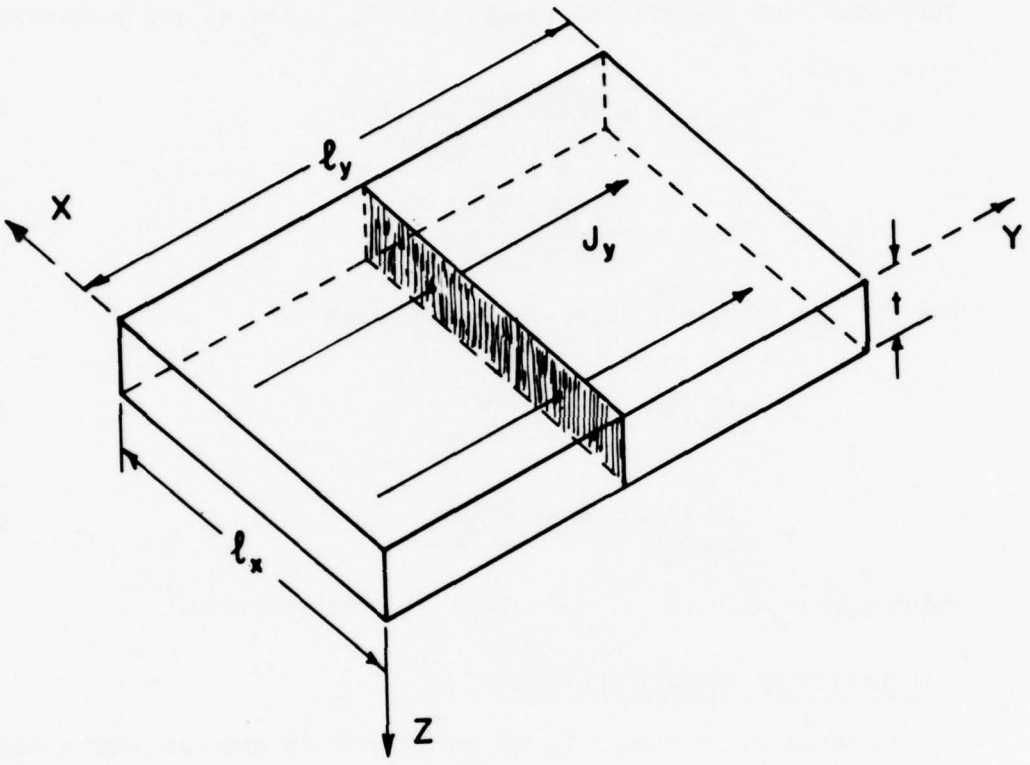

Figure 11. Rectangular Current Flow (skin effect)

where $W_t = W_R + W_\ell$ is the input power

W_R is the power radiated

W_ℓ is the power dissipated (in the equivalent resistances).

The power (input and dissipated) may be represented by a matrix, [W], where

$$W_i = \mathrm{Re}\ i_i v_i^* \tag{2-29}$$

In this representation, the typical element W_i is the input power to a port, positive if the port is driven, negative or zero if it is loaded, and zero if the port is metallic.

Then the input power W_t may be found by summing over the driven ports,

$$W_t = \sum_{\substack{\text{DRIVEN} \\ \text{PORTS}}} \mathrm{Re}\ i_i^* v_i \tag{2-30}$$

and the dissipated power W_ℓ may be found by summing over the loaded ports:

$$W_\ell = -\sum_{\substack{\text{LOADED} \\ \text{PORTS}}} \mathrm{Re}\ i_i^* v_i \tag{2-31}$$

Dissipated power may also be found by

$$W_\ell = \sum_{\substack{\text{LOADED} \\ \text{PORTS}}} (\mathrm{Re}\ z_{\ell i}) \left| i_i \right|^2 . \tag{2-32}$$

thus

$$\text{Efficiency} = \frac{W_t - W_\ell}{W_t} = \frac{\sum_{\substack{\text{DRIVEN} \\ \text{PORTS}}} \mathrm{Re}\ i_i^* v_i - \sum_{\substack{\text{LOADED} \\ \text{PORTS}}} (\mathrm{Re} z_{\ell i}) \left| i_i \right|^2}{\sum_{\substack{\text{DRIVEN} \\ \text{PORTS}}} \mathrm{Re}\ i_i^* v_i} \tag{2-33}$$

2.4 SCATTERING CHARACTERISTICS

Consider the scattering problem shown in Fig. 12a which shows a known electric field $\underline{E}^{inc}$ incident upon a rectangular plate of composite material. Fig. 12b shows the equivalent problem, a loaded wire-grid structure. All resistances are computed with the assumption of rectangular current flow (equations 2-15 and 2-16)

This problem may be represented ([1]), [3]) as a matrix equation of the following form

$$[-v^{(inc)}] = \left[[z] + [z_L]\right] [i] \tag{2-34}$$

where the typical element v_i^{inc} is a generalized incident voltage (an integral of the known incident electric field). Currents [i] are determined by matrix inversion. Scattered fields radiated by the wire-grid currents are obtained as in the radiation problem. The back-scattering cross section (echo area) is obtained [8] as

$$A_e = \text{echo area} = \lim_{r \to \infty} \left(4\pi r^2 \frac{S^s}{S^i}\right) \tag{2-35}$$

where S^s is scattered power density, at a distance of r from the scatterer, in the backward direction, and S^i is the incident power density.

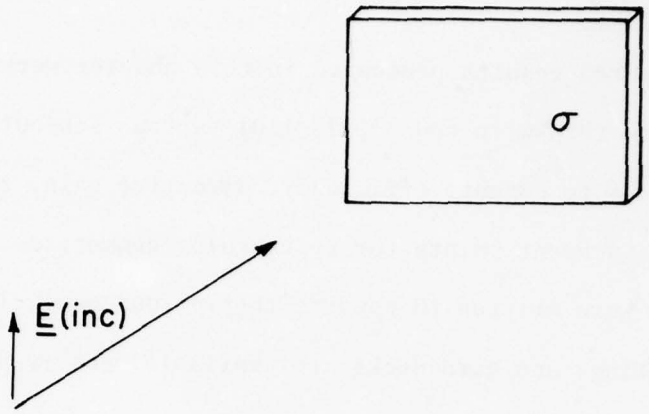

(a)

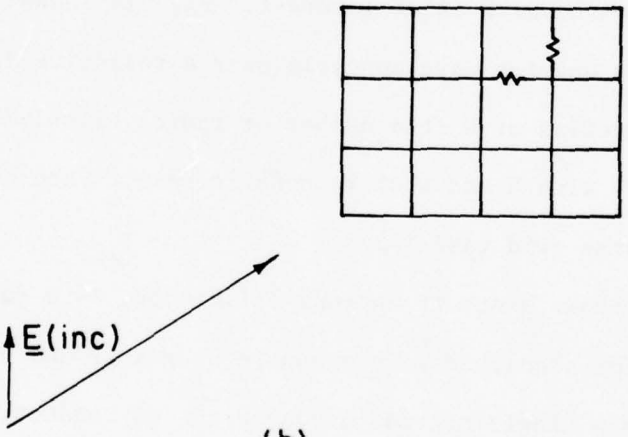

(b)

Figure 12. Back-scattering from Composite Material
(a) geometry (b) model

3.0 COMPUTED RESULTS

The computed results presented in this chapter were obtained by modifying two thin-wire codes [9], [10] various subroutines were added to these codes to compute efficiency, directive gain, echo area, and to handle attachment points for rectangular geometries. Additional subroutines were written to compute the various equivalent resistances. Program listings and card decks are available upon request to the authors.

3.1 PROBLEMS WITH AZIMUTHAL SYMMETRY (LOW-FREQUENCY CASE)

Fig. 13a, b show monopoles over a single section, double section composite ground plane, respectively, and indicate the parameters R, ℓ, R_1, σ_1, R_2, σ_2 used in this section of Chapter III.

In any wire-grid representation of a surface, the effect of the coarseness of the grid is of interest. Fig. 14 shows some typical results for a quarter wave monopole over a resistive disk of radius $\lambda/4$, as a function of N (the number of radial wires). Note that R_i varies slowly with N and that reasonable results are obtained even in the very-coarse grid case N=4.

Fig. 15 shows plots of antenna efficiency, as a function of conductivity, for a quarter-wave monopole over a ground plane. The lower curve is for a single-section ground plane of conductivity σ, radius λ. The upper curve shows the effect of replacing the central portion of the ground plane with a perfectly conducting pad of radius $R_1=0.5\lambda$. Note that antenna efficiency is increased for all values of conductivity σ.

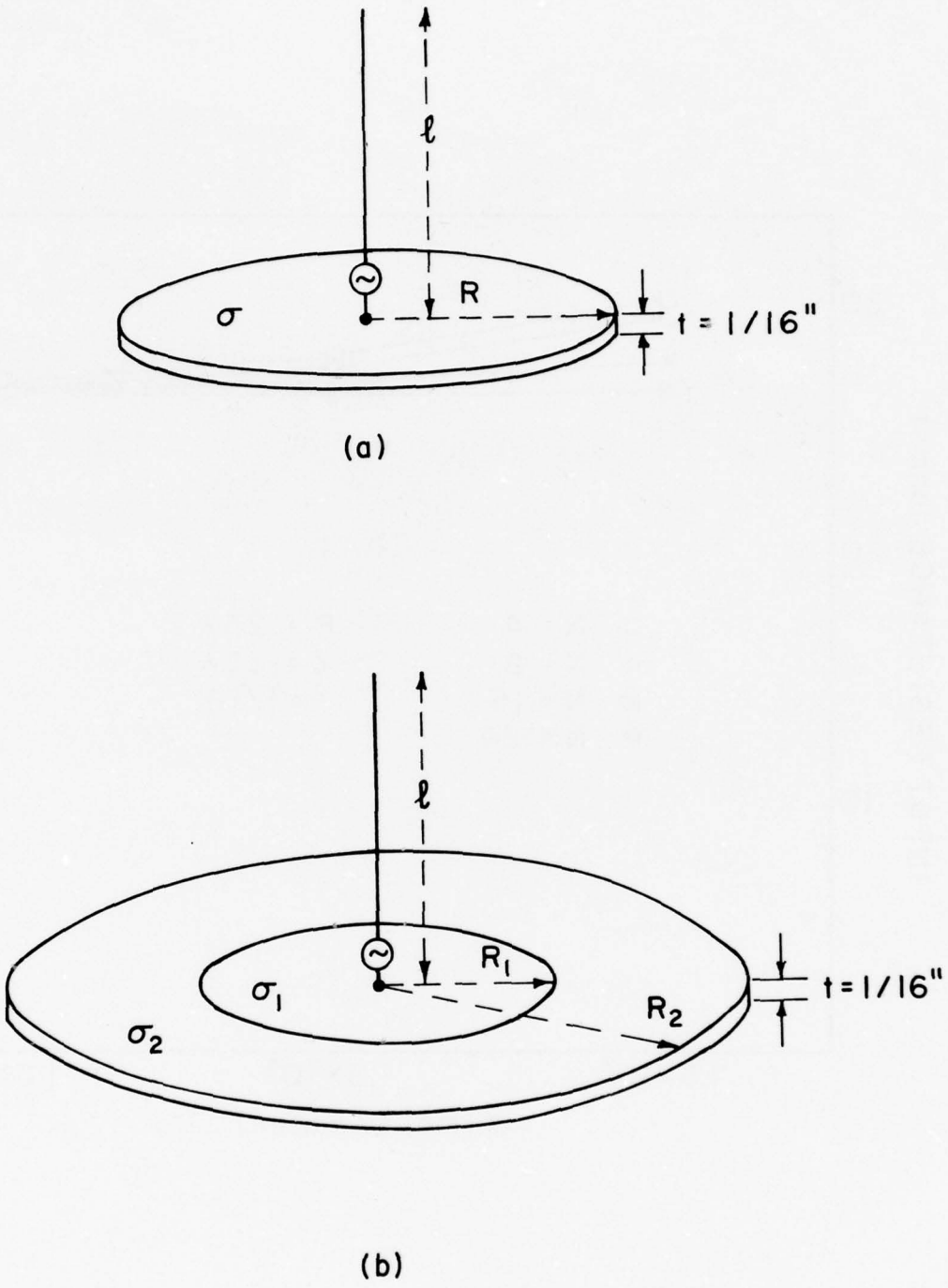

Figure 13. A Monopole Antenna over a Circular Composite Ground Plane (a) single ground plane section (b) double ground plane section

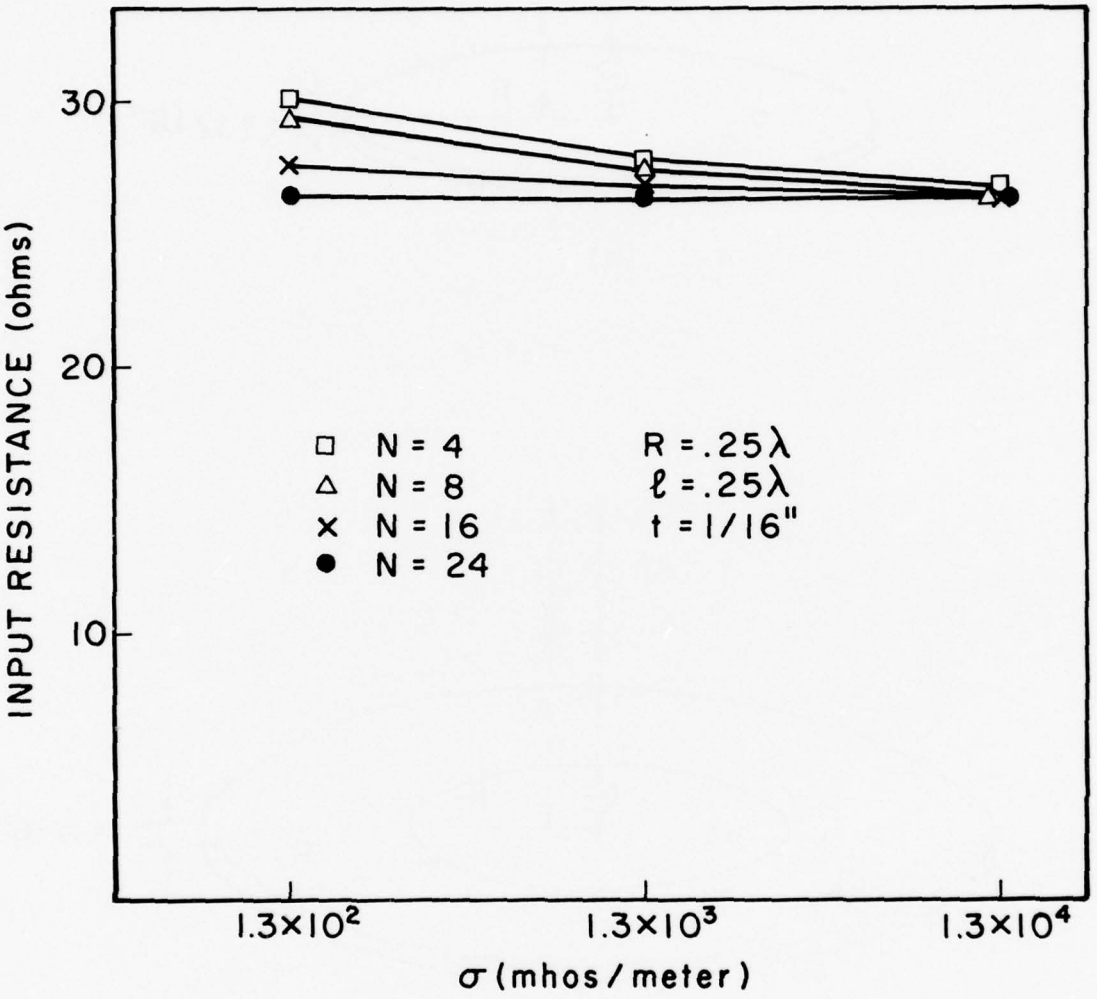

Figure 14. Variation of Input Resistance With the Number of Radial Wires

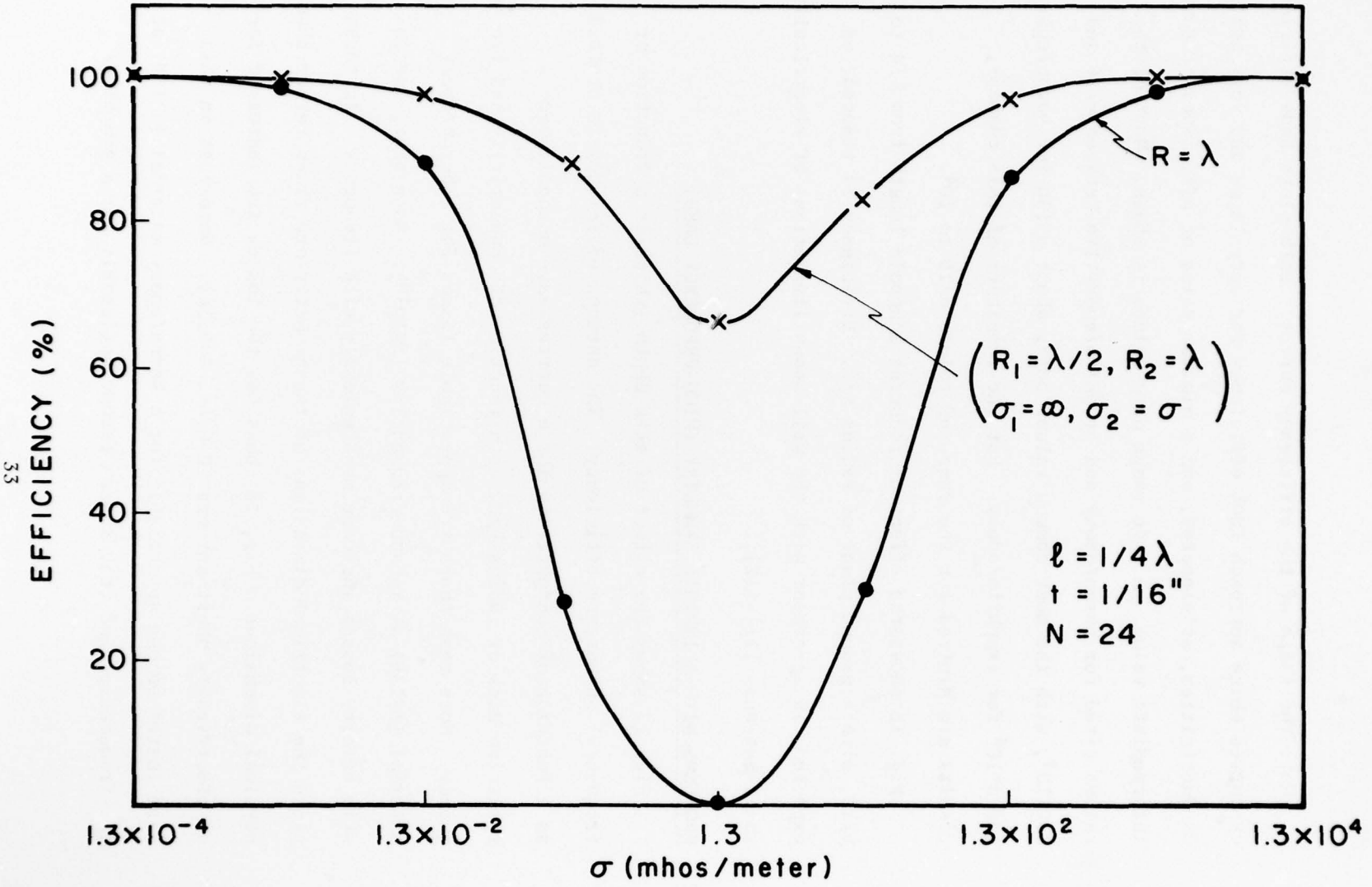

Figure 15. Improvement of Antenna Efficiency with Addition of a Conducting "Pad"

Note the shape of the efficiency curves. Both plots show efficiency curves which approach 100% efficiency for very large and very small conductivities, as expected, and a minimum value of efficiency at some intermediate value. A wide range of σ values is shown. Most of the values cited for boron/epoxy and graphite/epoxy lie between σ=10 and $\sigma=2\times10^4$, with the most common values being about $\sigma\approx130$ for boron/epoxy and $\sigma\approx10^4$ for graphite/epoxy. For the remainder of this chapter, results are plotted for the range of values σ=10 to 10^4.

Fig. 16 shows the effect of reducing monopole length from $\lambda/4$ to $\lambda/10$, with a ground plane of radius $\lambda/2$. Efficiency is reduced, as expected, in agreement with the well-known limitations of electrically small antennas [11]-[12].

3.2 PROBLEMS WITH AZIMUTHAL SYMMETRY (HIGH-FREQUENCY CASE)

Fig. 17 shows the effect of skin depth (which is a frunction of frequency) on antenna efficiency. The antenna efficiency is plotted as a function of conductivity for a quarter-wave monopole over a resistive disk of radius $\lambda/2$, as a function of conductivity and frequency. Note that there are appreciable losses for a boron/epoxy material ($\sigma\approx130$) at x-band frequencies ($f=10^{10}$). Note that, due to skin effect, losses increase monotonically with frequency. In these plots the electrical dimensions of the geometry are fixed rather than physical dimensions. Fig. 18 shows how the losses are increased for an electrically short antenna ($R=0.5\lambda$, $\ell=0.1\lambda$). Note that in this case losses become appreciable for a boron/epoxy material ($\sigma\approx130$) at low frequencies and that losses become noticeable for a graphite/

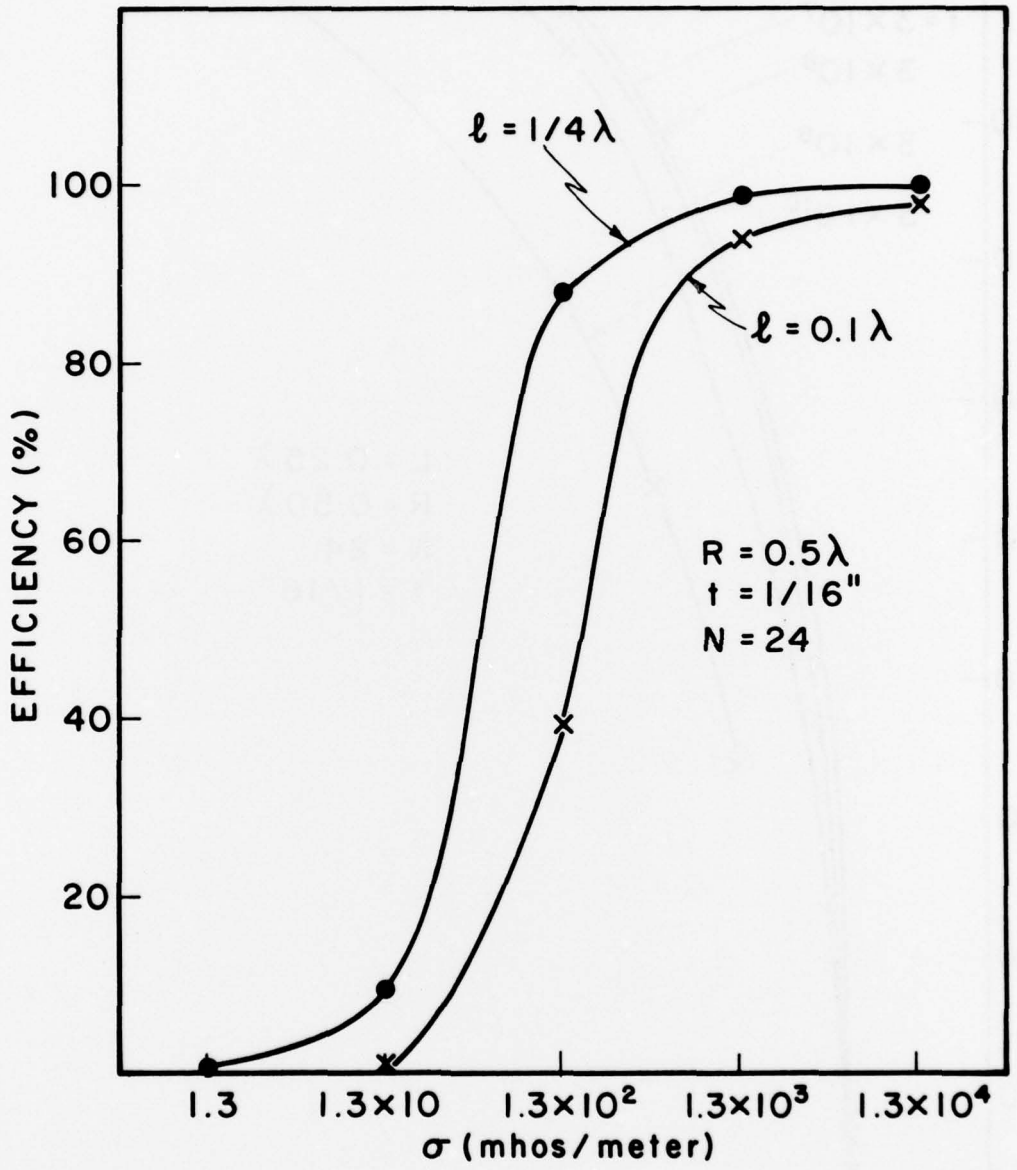

Figure 16. Effect of Antenna Length on Efficiency

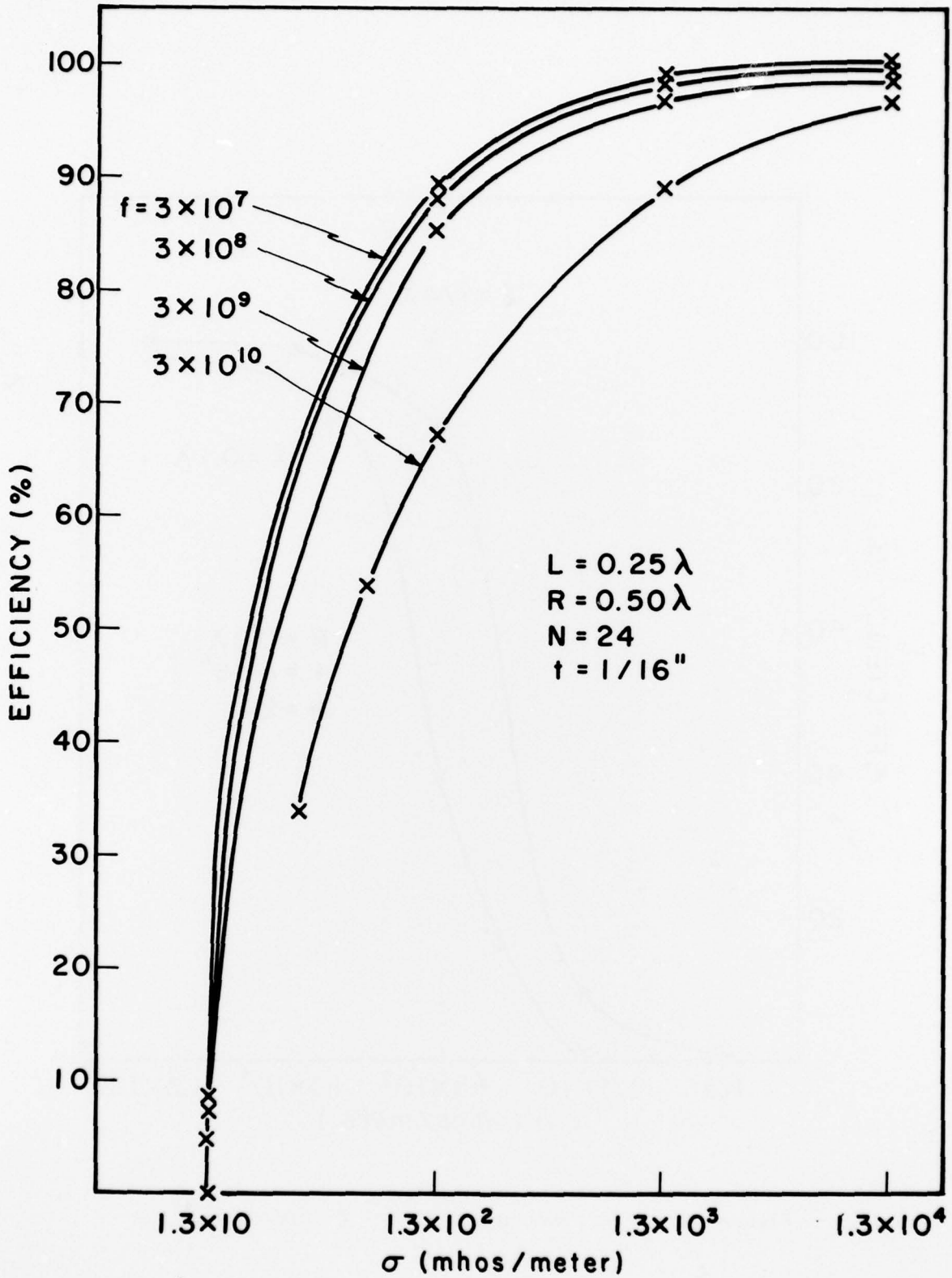

Figure 17. Effect of Skin Depth on Antenna Efficiency for Quarter Wave Monopole

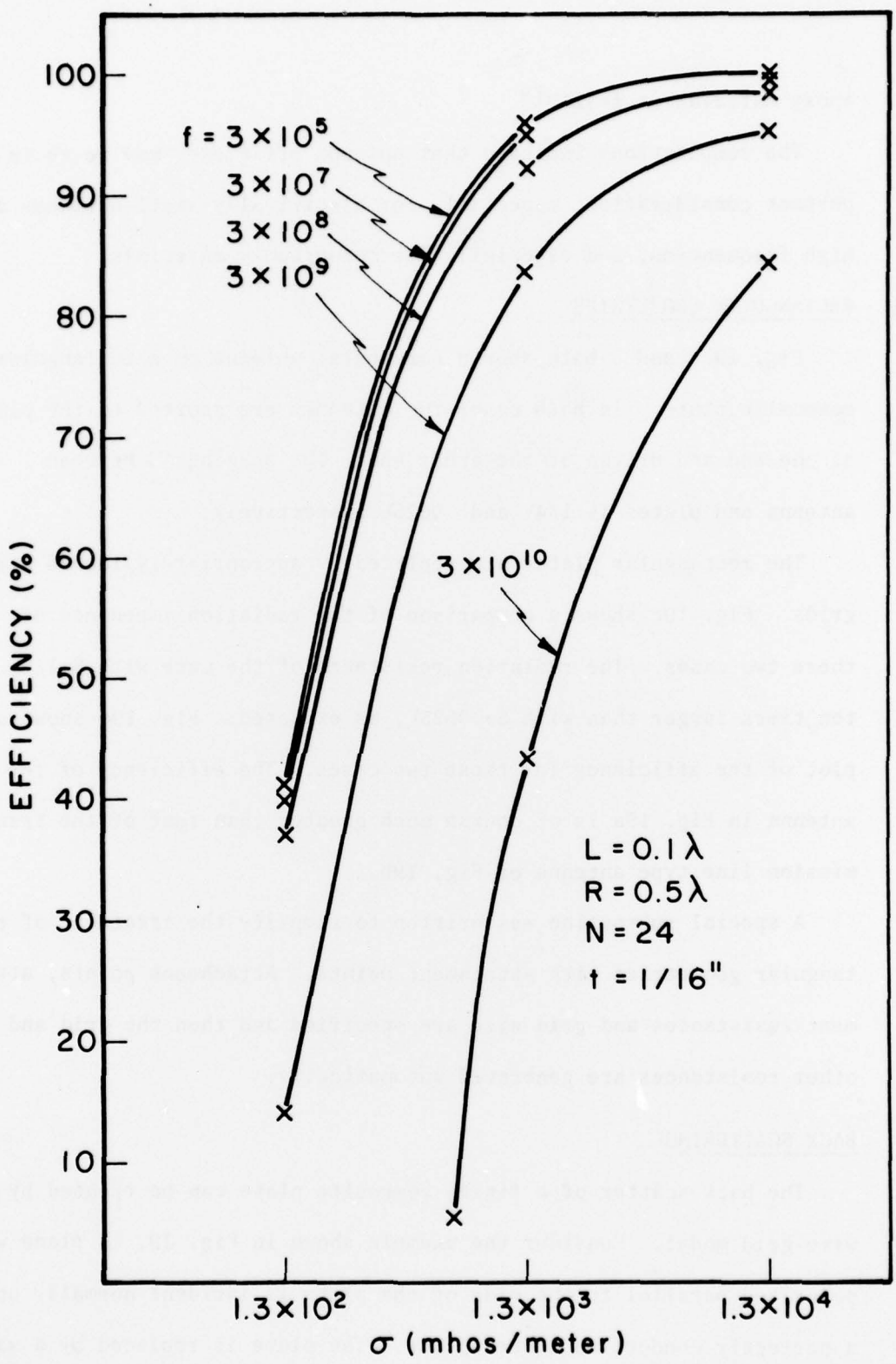

Figure 18. Effect of Skin Depth on Efficiency for a Short Monopole (ℓ=0.1λ)

epoxy material at $f=3x10^{10}$.

The computations indicate that antenna efficiency may be an important consideration, especially for electrically small antennas or high frequencies, and especially for boron/epoxy materials.

3.3 RECTANGULAR GEOMETRIES

Fig. 19 a and b both show a horizontal antenna on a rectangular composite plate. In both cases the antennas are shorted to the plate at one end and driven at the other end. The spacings S between antenna and plates is $1/4\lambda$ and $.0625\lambda$ respectively.

The rectangular plates are replaced by appropriately loaded wire grids. Fig. 19c shows a comparison of the radiation impedance of these two cases. The radiation resistance of the case with $S=1/4\lambda$ is ten times larger than with $S=.0625\lambda$, as expected. Fig. 19d shows a plot of the efficiency for these two cases. The efficiency of the antenna in Fig. 19a is of course much greater than that of the transmission line type antenna of Fig. 19b.

A special subroutine was written to simplify the treatment of rectangular geometries with attachment points. Attachment points, attachment resistances and grid size are specified and then the grid and other resistances are generated automatically.

3.4 BACK SCATTERING

The back scatter of a finite composite plate can be treated by a wire-grid model. Consider the example shown in Fig. 20. A plane wave polarized parallel to one side of the plate is incident normally upon a perfectly conducting square plate. The plate is replaced by a wire

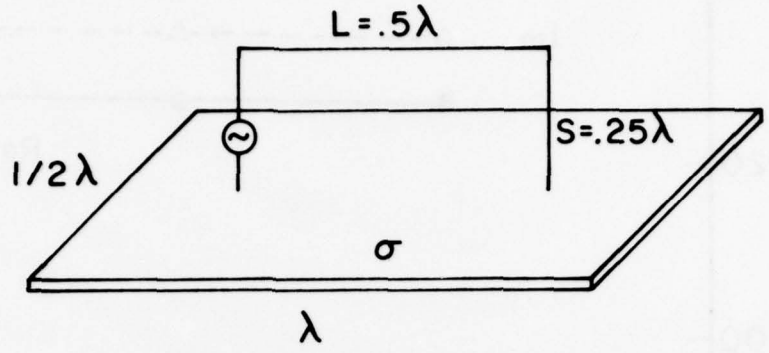

(a)

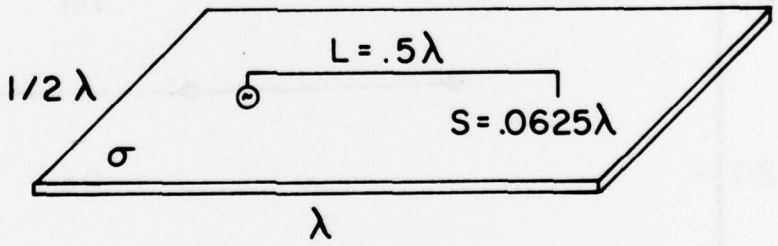

(b)

Figure 19. Antenna Over Composite Material (a) antenna 1 (b) antenna 2

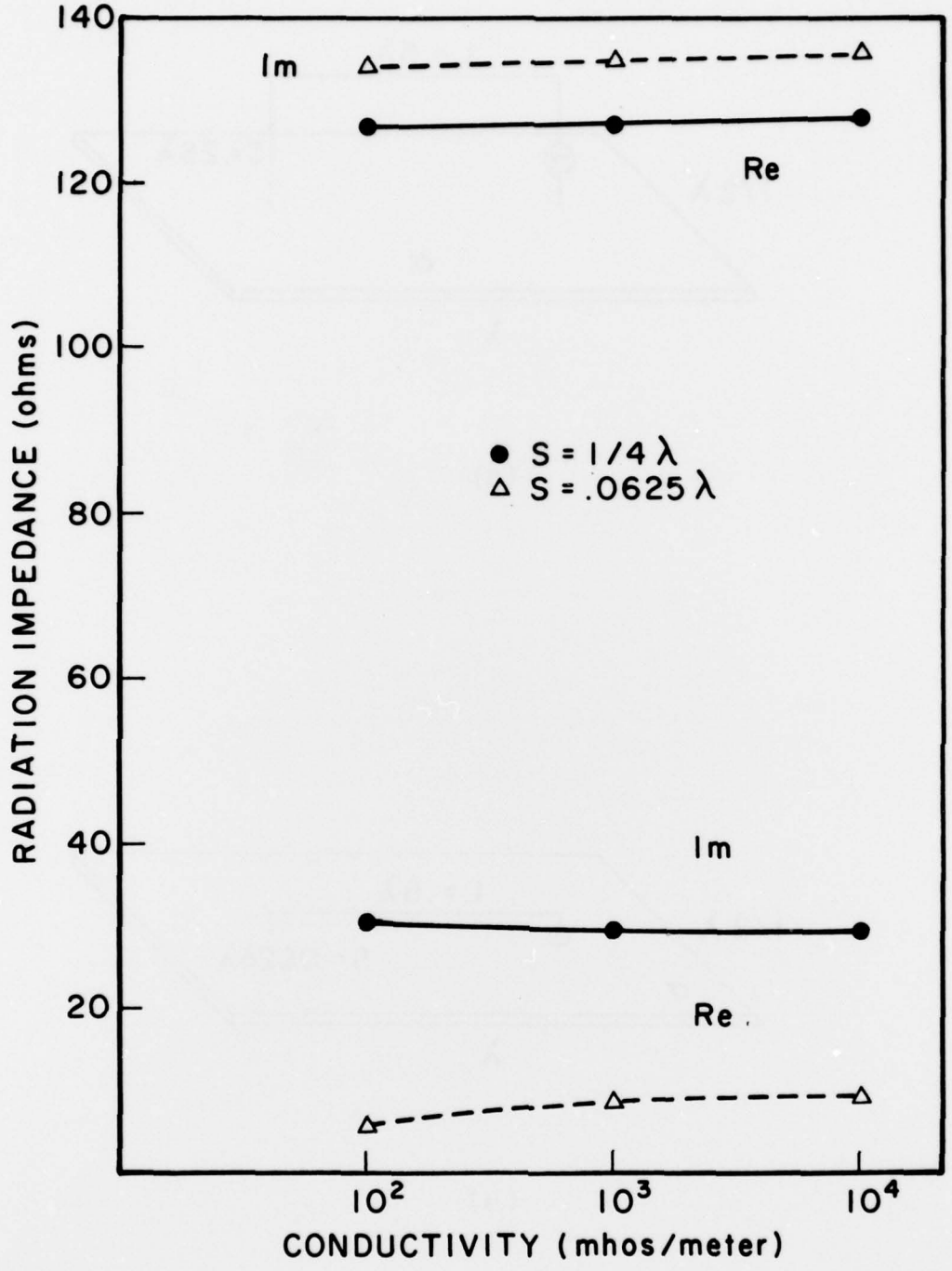

Figure 19. Antenna over composite material (c) impedance

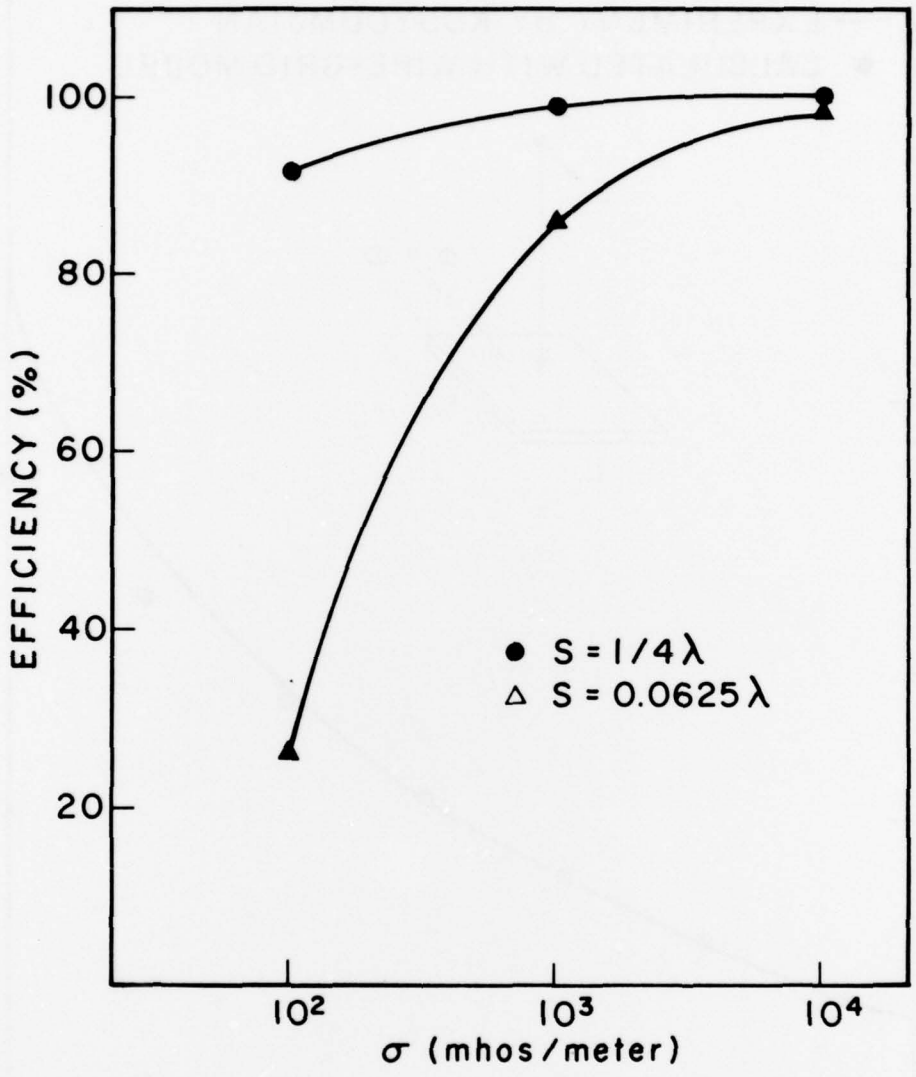

Figure 19. Antenna over Composite Material (d) efficiency

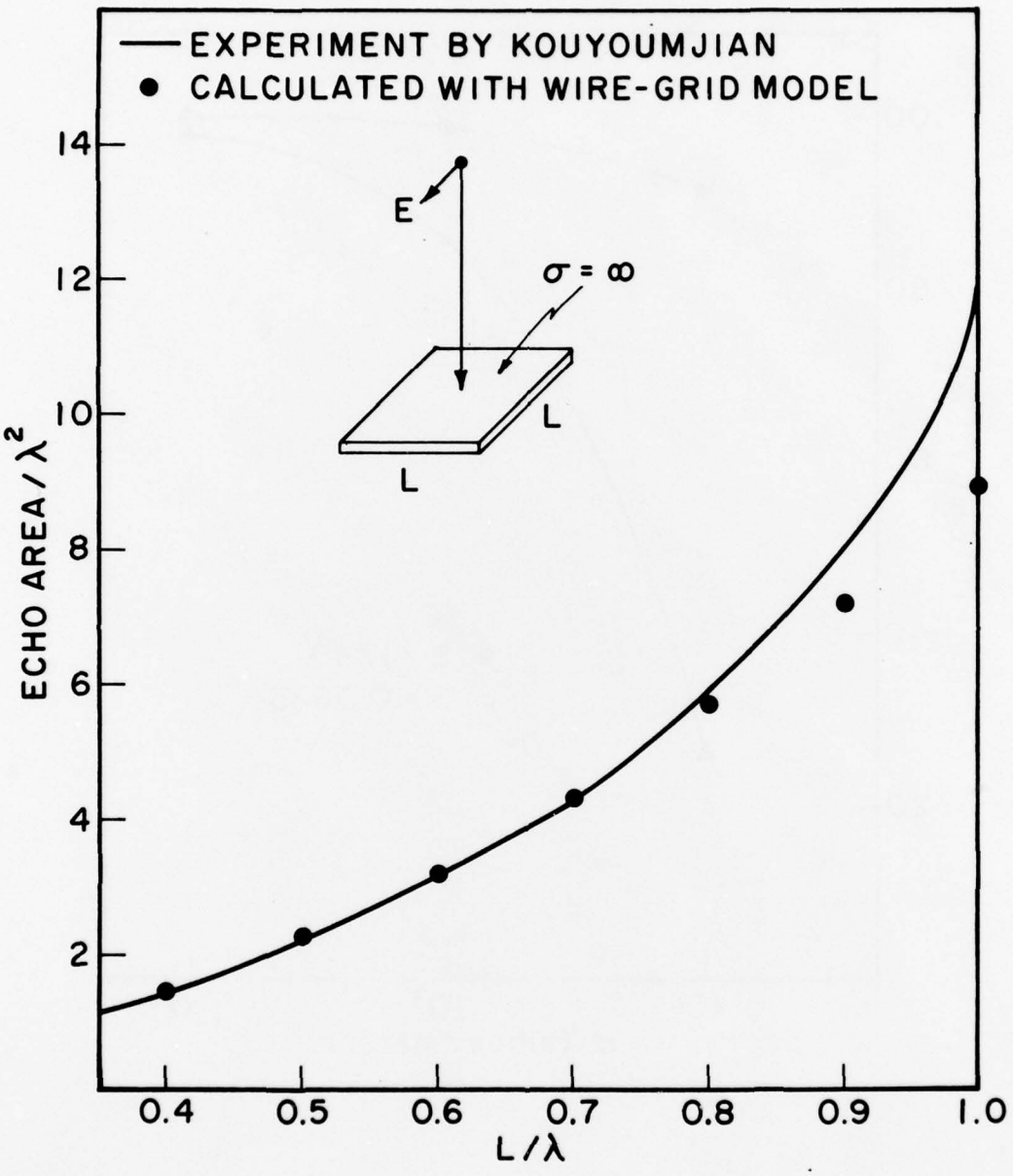

Figure 20. Echo Area of a Rectangular Perfect Conductor (normal incidence)

grid of appropriate size and shape. The electrical echo areas (A_e/λ^2) of different sizes of square plates are calculated. Fig. 20 shows a comparison of computed and experimental data for broadside echo area, for a perfectly conducting plate.

Consider the example shown in Fig. 21. A plane wave is normally incident upon a $\lambda/2$ by $\lambda/2$ lossy composite plate with conductivity σ. The lossy plates are replaced by appropriately loaded wire grids. Fig. 21 shows a plot of the electrical echo area against conductivity. The echo areas approach the perfect conducting asymptote for the cases with conductivity greater than 10^4 and approach zero for the cases with conductivity less than 10^{-1}. Beam patterns have also been plotted for the cases of Fig. 21. They show very little change in the beam patterns as the echo area changes by a factor greater than ten.

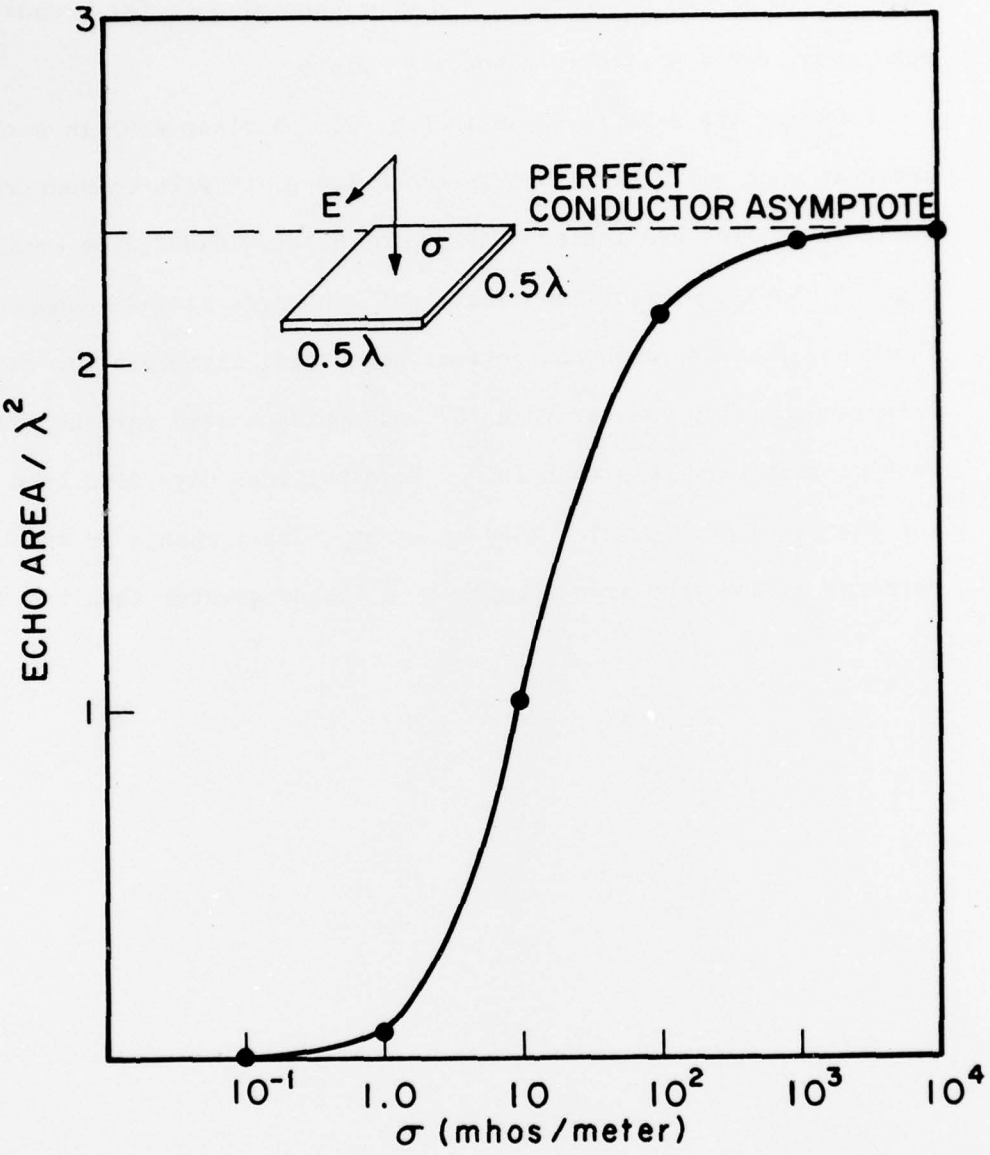

Figure 21. Echo Area of a Lossy Rectangular Section (normal incidence)

4.0 CONCLUSIONS

Loaded thin-wire models have been developed for the representation of the electromagnetic properties of advanced composite materials. These models apply especially to radiation properties of antennas over composite surfaces and back-scattering from composites. Special techniques are required for attachment points. Skin depth is taken into account. Antenna efficiency and gain are computed. A small metal pad antenna efficiency may be an important consideration for boron/epoxy, especially for electrically small antennas. A small metal "pad" at attachment points may significantly improve efficiency. Finally, far field beam patterns may remain essentially unchanged as efficiency or back scatterer varies over a wide range.

REFERENCES

[1] R. F. Harrington, Field Computation by Moment Methods, Macmillan Co, NY, 1978.

[2] R. F. Harrington, "Matrix Methods for Field Problems", Proc. IEEE vol. 55, pp. 136-149, Feb. 1967.

[3] A. T. Adams, "An Introduction to the Method of Moments", RADC-TR-73-217, Vol I, Nov. 1974, 916421L.

[4] J. L. Allen et al, "Electromagnetic Properties and Effects of Advanced Composite Materials: Measurement and Modeling", RADC-TR-78-156, June 1978, A058041.

[5] J. L. Allen et al, "A Technology Plan for Electromagnetic Characteristics of Advanced Composites", RADC-TR-76-206, July 1976, A030507.

[6] R. F. Harrington, Time-Harmonic Electromagnetic Waves, McGraw-Hill, NY, 1961, p. 53.

[7] IBID, p. 22.

[8] IBID, p. 116.

[9] D. E. Warren et al, "Electric and Magnetic Fields of Wire Antennas", IEEE Trans. on Antennas and Propagation, Vol. Ap-22, No. 2, March 1974, p. 364. Program on deposit with NAPS (ASIS-NAPD DOCUMENT No. NAPS-02221).

[10] Computer Code MBA-L^3-1B, Lawrence Livermore Laboratory, Livermore, California (See WAMP: A User's Manual for the Wire Antenna Modeling Program by F. J. Deadrick and E. K. Miller, Lawrence Livermore Laboratory Report, UCID-30084, Dec. 10, 1973).

MISSION
of
Rome Air Development Center

RADC plans and conducts research, exploratory and advanced development programs in command, control, and communications (C^3) activities, and in the C^3 areas of information sciences and intelligence. The principal technical mission areas are communications, electromagnetic guidance and control, surveillance of ground and aerospace objects, intelligence data collection and handling, information system technology, ionospheric propagation, solid state sciences, microwave physics and electronic reliability, maintainability and compatibility.